# DISSIMILAR METAL WELDING OF INCONEL 718 WITH TI6AL4V: A SIMULATION-BASED APPROACH USING CATIA

**A PROJECT REPORT**

**Submitted by**

**ARUN K S**

**REG. No.: TKM21MECI06**

**to**

**The APJ Abdul Kalam Technological University**

**in partial fulfilment of the requirements for the award of Degree**

**of**

**Master of Technology**

**in**

***Computer Integrated Manufacturing***


**DEPARTMENT OF MECHANICAL ENGINEERING**

**T K M College of Engineering, Kollam**

**JULY 2023**

# DECLARATION

I, **ARUN K S** hereby declare that, this project report **"DISSIMILAR METAL WELDING OF INCONEL 718 WITH TI6AL4V: A SIMULATION-BASED APPROACH USING CATIA"** submitted for the partial fulfillment of the requirements for the award of degree of Master of Technology of the APJ Abdul Kalam Technological University is a bonafide work done by me under the supervision of **Dr. ANAND SEKHAR R.**, Asst. Professor, TKM College of Engineering, Kollam. This submission represents my ideas in my own words and where ideas or words of others have also been included. I have adequately and accurately cited and referenced the original sources. I also declare that I have adhered to ethics of academic honesty and integrity and have not mispresented or fabricated any data or idea of fact or source in my submission. I understand that any violation of the above will be a cause for disciplinary action by the institute and/or the University and can also evoke penal action from the sources which have thus not been properly cited or form whom proper permission has not been obtained. This report has not been previously formed the basis for the award of any degree, diploma or similar title of any other University.

Signature:

**Name of the student: ARUN K S**

**Register No.: TKM21MECI06**

Kollam

Date: 12/07/2023

**DEPARTMENT OF MECHANICAL ENGINEERING**

**TKM COLLEGE OF ENGINEERING, KOLLAM**

## CERTIFICATE

This is to certify that the project entitled **"DISSIMILAR METAL WELDING OF INCONEL 718 WITH Ti6Al4V: A SIMULATION-BASED APPROACH USING CATIA"** submitted by **ARUN K S, (TKM21MECI06)** during **2021-23** to the APJ Abdul Kalam Technological University in partial fulfillment of the requirements for the award of the Degree of Master of Technology in Computer Integrated Manufacturing, Mechanical Engineering is a Bonafede record of the project work carried out by him under our guidance and supervision. This report in any form has not been submitted to any other University or Institute for any purpose.

18/7/23

**Dr. ANAND SEKHAR R.**
Internal Project Supervisor
Assistant Professor
Dept. of Mechanical Engineering
TKM College of Engineering, Kollam

PG Cordinator:
**Prof. KANNAN S**
Assistant Professor
Dept. of Mechanical Engineering
TKM College of Engineering, Kollam

18/7

**Dr. P. N. Dileep**
Head of the Department
Dept. of Mechanical Engineering
TKM College of Engineering, Kollam

# ACKNOWLEDGEMENT

I take this opportunity to express my deep sense of gratitude and sincere thanks to all who helped me to complete the project successfully.

I am greatly thankful to **Dr. T.A. Shahul Hameed**, Principal, TKM College of Engineering, and **Dr. Dileep P.N.**, Head of Mechanical Engineering Department for their support and cooperation.

I am deeply indebted to my guide **Dr. ANAND SEKHAR R**, Asst. Professor, Department of Mechanical Engineering for his excellent guidance, positive criticism, and valuable comments.

My heartfelt gratitude to **Prof. Kannan S.**, PG coordinator, Department of MechanicalEngineering, and **Prof. Faizal N.S.**, Assistant Professor, Department of Mechanical Engineering for their valuable suggestions and guidance in the preparation of the project presentation and report.

I also express my thanks to the teaching and non-teaching staff of T.K.M. College of Engineering who have supported us in the successful completion of our project.

I will be failing in duty if I do not acknowledge with thanks to the authors of the references andother literature referred to this project.

Finally, I thank my parents, friends, and near and dear ones who directly and indirectly contributed to the successful completion of my project.

Kollam

12/07/2023 **ARUN K S**

# ABSTRACT

Dissimilar metal welding, particularly the joining of Inconel 718 and Ti-6Al-4V alloys, presents significant challenges due to their disparate properties. This study proposes a simulation-based approach for Tungsten Inert Gas (TIG) welding of Inconel 718 with Ti6Al4V using the Computer-Aided Design (CAD) software CATIA. The objective is to investigate the feasibility of achieving high-quality weld joints with minimized defects and optimized process parameters.

The simulation process commences with the development of a three-dimensional (3D) model of the welding setup in CATIA. The model accurately represents the geometry of the weld joint, encompassing the base materials. Subsequently, mechanical analysis is performed to evaluate the deformation, Von Mises, displacement and principal stress under the applied load of 100 N for Inconel 718 and Ti6Al4V.

The experimental procedure provided valuable insights into the weldability and the formation of intermetallic compounds responsible for the quality of joints between Inconel 718 and Ti6Al4V. The results obtained from this study can contribute to the optimization of welding parameters and the development of reliable welding procedures for joining these high-performance alloys in various industrial applications requiring excellent corrosion resistance, high-temperature strength, and mechanical integrity.

# CONTENTS

# LIST OF FIGURES

Title Page Number

# LIST OF TABLES

**Title** **Page Number**

# CHAPTER 1
# INTRODUCTION

The need for high-performance materials and their efficient joining methods has increased dramatically in the field of modern engineering. The method of dissimilar metal welding, which includes joining two distinct metals, has become essential for achieving improved mechanical qualities and usefulness in numerous sectors. This study seeks to investigate the weld joint properties using simulation techniques in ANSYS and explore the dissimilar metal welding of two commonly used alloys, Inconel 718 and Ti6Al4V.

## 1.1 INCONEL 718

Inconel 718, a nickel-based superalloy, has emerged as a highly sought-after material in various industries due to its exceptional mechanical properties and resistance to extreme conditions [1]. Developed in the 1950s, Inconel 718 has become widely recognized for its excellent high-temperature strength, corrosion resistance, and remarkable weldability. This alloy has found extensive applications in aerospace, power generation, oil and gas, and chemical processing industries [13].

The unique combination of properties exhibited by Inconel 718 makes it particularly suitable for applications that demand strength and durability at elevated temperatures [2]. The alloy maintains its mechanical integrity even when exposed to harsh environments characterized by high temperatures, pressure, and corrosive elements. This makes it an ideal choice for components subjected to extreme conditions, such as gas turbine engines, rocket motors, nuclear reactors, and various chemical processing equipment [1].

One of the key factors contributing to the popularity of Inconel 718 is its high-temperature strength. The alloy retains its strength even at temperatures exceeding 650°C (1,200°F), allowing it to withstand significant mechanical stresses in demanding applications. This

characteristic makes Inconel 718 highly desirable in applications where other materials may deform or lose their strength under extreme thermal conditions [9].

Corrosion resistance is another noteworthy attribute of Inconel 718. The alloy demonstrates exceptional resistance to a wide range of corrosive environments, including acids, alkalis, and chloride solutions. This corrosion resistance, combined with its high-temperature strength, makes Inconel 718 well-suited for components exposed to aggressive chemical environments, such as downhole oil and gas drilling equipment, chemical processing vessels, and marine applications [13].

Furthermore, Inconel 718 exhibits excellent weldability, making it a preferred choice for fabricating complex structures and joining dissimilar metals. The alloy can be readily welded using various conventional welding techniques, including gas tungsten arc welding (GTAW), shielded metal arc welding (SMAW), and electron beam welding (EBW). Its weldability, coupled with its ability to maintain strength and resistance to corrosion in the welded regions, enables the fabrication of intricate and robust assemblies.

The exceptional properties of Inconel 718 have spurred extensive research and development efforts to further enhance its performance and explore new applications. Researchers and engineers continually investigate its behavior under different processing conditions, such as heat treatment, casting, and additive manufacturing methods [15]. Moreover, advancements in simulation techniques, such as finite element analysis (FEA) and computational thermodynamics, enable a deeper understanding of Inconel 718's behavior and facilitate the optimization of its properties for specific applications.

### 1.2 Ti-6Al-4V

Ti-6Al-4V or Grade 5 titanium, is a widely recognized and extensively used titanium alloy renowned for its exceptional combination of mechanical properties, corrosion resistance, and biocompatibility. Composed of 90% titanium (Ti), 6% aluminum (Al), and 4% vanadium (V),

Ti6Al4V has become a material of choice in various industries, including aerospace, biomedical, automotive, and chemical processing [3].

The unique composition of Ti6Al4V provides it with remarkable mechanical properties. It offers a high strength-to-weight ratio, exceeding that of most other engineering materials. This attribute, along with its low density, allows for the fabrication of lightweight components that can withstand significant mechanical loads. As a result, Ti6Al4V has become a preferred choice in aerospace applications, where weight reduction is critical for enhancing fuel efficiency and overall performance [10].

In addition to its strength, Ti6Al4V possesses excellent corrosion resistance. It forms a protective oxide layer on its surface, rendering it highly resistant to a wide range of corrosive environments, including seawater and various acids. This corrosion resistance makes Ti6Al4V suitable for applications where exposure to aggressive chemical environments is expected, such as chemical processing equipment and marine components [17].

Another distinguishing feature of Ti6Al4V is its biocompatibility. The alloy is widely used in the biomedical field for implants and prosthetic devices due to its ability to integrate well with human tissues and exhibit excellent resistance to corrosion within the human body. This biocompatibility, coupled with its mechanical properties, has led to successful applications in dental implants, joint replacements, and medical instruments.

Ti6Al4V also demonstrates excellent resistance to fatigue and fracture, making it suitable for components subjected to cyclic loading and high-stress conditions. This attribute is crucial in industries such as automotive and sporting goods, where components undergo repetitive stress and require long-lasting performance.

Moreover, Ti6Al4V exhibits good weldability, enabling the fabrication of complex structures and the joining of components using various welding techniques. This characteristic, along

with its favourable mechanical properties, contributes to its versatility and broad application potential.

As a result of its outstanding properties, Ti6Al4V continues to be a subject of extensive research and development. Efforts are focused on optimizing its properties through advanced manufacturing techniques such as additive manufacturing, which enables the production of complex geometries and customized designs with enhanced performance.

## 1.3 TIG WELDING

Tungsten Inert Gas (TIG) welding, also known as Gas Tungsten Arc Welding (GTAW), is a versatile and widely used welding process known for its precision, high-quality welds, and versatility in joining a wide range of materials. TIG welding utilizes a non-consumable tungsten electrode, an inert gas shield, and a filler material (if needed) to create a strong and reliable fusion between metal parts [2].

The TIG welding process relies on the heat generated by an electric arc formed between the tungsten electrode and the workpiece. The tungsten electrode remains non-consumable throughout the process, serving as a stable heat source [3]. The arc is shielded from atmospheric contamination by an inert gas, typically argon or helium, which is directed through a nozzle surrounding the electrode.

One of the significant advantages of TIG welding is its ability to produce high-quality, precise welds. The process allows for exceptional control over the heat input, arc length, and welding speed, resulting in welds with minimal distortion, low spatter, and superior visual appearance. This level of control makes TIG welding particularly suitable for applications where aesthetics and weld quality are paramount, such as in the aerospace, automotive, and food processing industries [8].

TIG welding offers excellent versatility in terms of the materials it can join. It can be used to weld a wide range of metals, including stainless steel, aluminum, titanium, copper, and nickel alloys. This versatility makes TIG welding a preferred choice in applications that require joining dissimilar metals or materials with different thicknesses, as it provides the necessary control and adaptability to achieve strong and reliable welds [11].

Furthermore, TIG welding is known for its ability to produce welds with minimal heat input, reducing the risk of distortion and damage to heat-sensitive materials. This characteristic makes it suitable for thin-gauge materials and delicate components, as well as for welding applications where heat-affected zone (HAZ) control is critical, such as in the welding of heat-treated or corrosion-resistant alloys.

TIG welding is widely used in various industries, including automotive, aerospace, petrochemical, and manufacturing, where high-quality welds and precise control are essential [5]. The process finds applications in the fabrication of pipes, pressure vessels, aircraft components, automotive exhaust systems, and intricate metalwork.

## 1.4 CATIA SOFTWARE

The analysis of welding using CATIA, a leading software suite for computer-aided design (CAD), computer-aided manufacturing (CAM), and computer-aided engineering (CAE), has revolutionized the way engineers and designers evaluate the performance and integrity of welded structures. Welding is a fundamental joining process used extensively in various industries, such as automotive, aerospace, construction, and shipbuilding. Understanding the behavior of welded components under different loading conditions is crucial for ensuring their structural integrity and optimal performance [33].

CATIA provides a comprehensive set of analysis tools that enable engineers to simulate and analyze welding processes, assess the thermal and structural effects, predict potential defects, and optimize welding sequences. These capabilities empower engineers to make informed

decisions during the design and manufacturing stages, leading to improved quality, reduced costs, and enhanced efficiency.

One of the key analysis techniques employed in CATIA for welding is Finite Element Analysis (FEA). FEA allows engineers to model and simulate the behavior of welded joints by dividing the component into finite elements and analyzing their interactions. By considering factors such as material properties, welding parameters, and loading conditions, FEA helps determine critical parameters like stress, strain, displacement, and deformation. This information aids in assessing the structural integrity and performance of the weldment.

Another critical aspect of welding analysis in CATIA is the simulation of the thermal effects. Welding processes generate intense heat, which can lead to thermal distortions, residual stresses, and potential defects. CATIA's thermal analysis capabilities enable engineers to evaluate the temperature distribution, cooling rates, and the influence of welding parameters on the material behavior [33]. This knowledge allows for the optimization of welding parameters and the design of appropriate pre-heating and cooling strategies to mitigate the adverse effects of welding-induced thermal cycles.

Additionally, CATIA offers fatigue analysis tools specifically tailored for welded structures. Welded joints are often subjected to cyclic loading, leading to fatigue failure if not properly evaluated. CATIA's fatigue analysis considers factors such as stress concentration, material properties, welding imperfections, and loading conditions to predict the fatigue life of welded components [33]. This knowledge aids in designing weldments that meet the required durability and reliability standards.

Furthermore, CATIA allows for the analysis of the strength and structural integrity of welded components. It enables engineers to assess the influence of weld size, joint configuration, material properties, and loading conditions on the overall performance of the weldment. By conducting strength and structural analysis, potential design flaws or areas of weakness can be

identified and addressed early in the design process, ensuring that the final welded structure meets the desired performance criteria.

## 1.5 WELDING OF INCONEL 718 WITH Ti-6Al-4V.

The superalloy Inconel 718, which is based on nickel, has great weldability, corrosion resistance, and high-temperature strength. It has several uses in the chemical, nuclear, and aerospace industries. However, the titanium alloy Ti6Al4V is a good choice for aerospace, medical, and automotive applications due to its outstanding strength-to-weight ratio, excellent biocompatibility, and strong corrosion resistance.

Due to the large variations in their physical and metallurgical properties, welding Inconel 718 with Ti6Al4V presents a difficult task. These discrepancies, such as those in melting temperatures, solidification behaviors, and thermal expansion coefficients, can cause brittle intermetallic phases to develop during welding as well as thermal stresses. Therefore, it is crucial to have a thorough grasp of the welding process and how it affects the joint's structural integrity.

Computer-aided simulations offer a useful tool to solve these difficulties and improve the dissimilar metal welding process. A popular finite element analysis program called ANSYS provides comprehensive capabilities for simulating and examining intricate welding events. This project uses CATIA to model the welding of Inconel 718 and Ti6Al4V dissimilar metals, anticipate the development of intermetallic compounds, assess residual stresses and distortions, and optimize welding settings for a defect-free weld connection.

# CHAPTER 2
# LITERATURE REVIEW

K.H. Song, et al [1] studied the friction-stir-welding and post-heat-treated Inconel 718 alloy and made the conclusion on mechanical and microstructural behaviour of the alloy. At a welding speed of 150 mm/min, they successfully completed FSW on the Inconel 718 alloy without creating any weld flaws. As a result, the use of FSW caused dynamic recrystallization to occur along with grain refinement from 10*10–6 m on average in the base material to 1-3*10–6 m in the stir zone. The mechanical properties of the grain were effectively improved and enhanced by this grain refining; the microhardness increased dramatically from 273 HV in the base material to 352 HV in the stir zone. Additionally, the tensile strength increased from the base material's 886 MPa to the stir zone's 1135 MPa, indicating a fracture in the base material at the joint. Furthermore, post-heat treatment improved the mechanical qualities.

K. Devendranath Ramkumar, et al [2] studied the weldability, microstructure and mechanical properties of activated flux TIG welding of Inconel 718.Their study addressed the successful joining of Inconel 718 using SiO2 and TiO2 flux assisted GTA welding process. The outcomes drawn from their study was Both SiO2 and TiO2 flux resulted in complete penetration while employing 140 A current, which was due to the arc constriction effect hence, these fluxes could be employed for joining Inconel 718 plates. The presence of laves phase was observed at the inter-dendritic regions of the fusion zone. The amount of laves phase was comparatively lesser in TiO2 flux assisted welding. The average fusion zone hardness was slightly greater for both the weldments compared to the base metal. The moderate cooling and low heat input due to high energy density of the A-TIG welding resulted in better hardness values. It was also noticed that during the tensile studies the fracture had occurred at the parent metal for both the weldments. Both SiO2 and TiO2 flux assisted weldments showcased better tensile properties compared to the parent metal and the impact toughness of the weldments obtained from the A-TIG welding process was due to the presence of inclusions in the fusion zone. Additionally, it was discovered that for both weldments, the fracture had happened at the parent metal during the tensile studies. The impact toughness of the weldments produced by

the A-TIG welding technique was caused by the presence of inclusions in the fusion zone, and both SiO2 and TiO2 flux assisted weldments displayed greater tensile qualities than the parent metal.

Guangxu Yan, et al [3] studied the mechanical properties of TIG welding Ti-6Al-4V and the difference on post heat treatment. Their investigation focused on how the PWHT affected the mechanical characteristics of Ti-6Al-4V that had just been welded. They found that while PWHT at 700 °C for 1 hour on as-welded Ti-6Al-4V decreases residual stresses to nearly 0 MPa, it has no discernible impact on the microstructure and micro-hardness. As the residual stresses reduce, the weld metal's yield strength rises by about 2.1%, and under fatigue loads ranging from 750 MPa to 950 MPa, its low cycle tensile fatigue life nearly equals that of the Ti-6Al-4V as received. For the as-welded Ti-6Al-4V, the PWHT at 700 °C for 1 hour can successfully minimize residual stresses, improving the fatigue life without degrading tensile strength or micro-hardness.

Xiao-Long Gao, et al [4] studied the dissimilar metal welding of Ti6Al4V and Inconel 718 through pulsed laser welding. In their research work Nb was utilized as an interlayer to avoid the Ti6Al4V alloy and Inconel 718 mixing, which prevented the formations of Ti-Ni, Ti-Cr, and Ti-Fe brittle intermetallics in the Ti6Al4V/Nb/Inconel 718 dissimilar joint. Two welding mechanisms were identified in the Ti6Al4V/Nb/Inconel 718 dissimilar joint. They utilized Fusion welding to join Ti6Al4V to niobium, whereas a eutectic reaction was utilized for the joining at the Inconel 718/Nb interface. The microstructure near the interface between Ti and Nb comprised of the columnar grains and the island areas, whereas no intermetallics formed in the FZ. Moreover, the Nb content was higher in the island areas than in the columnar grains. The eutectic reaction layer was formed at the Nb/Inconel 718 interface displaying the main microstructure of Ni-Nb system intermetallics. In the dissimilar joint, the reaction layer demonstrated relatively higher microhardness values compared to other regions, due to the NbNi3 and Nb7Ni6 formations. The tensile testing results demonstrated that the dissimilar joint fractures occurred in the reaction layer. Also, the tensile strength and the elongation of the dissimilar joint were 145 MPa and 1.2%, respectively. The major microstructure of the Ni-Nb system intermetallics was seen in the eutectic reaction layer that formed at the Nb/Inconel 718 contact. Due to the development of NbNi3 and Nb7Ni6, the reaction layer in the dissimilar

joint showed considerably greater microhardness values than other areas. The findings of the tensile tests showed that the response layer is where the different joint fractures happened. Additionally, the dissimilar joint's tensile strength and elongation were 145 MPa and 1.2%, respectively.

K. C. Ganesh, et al [5] studied the TIG Welding of AISI 316LN Stainless Steel, and studied the thermos mechanical properties. In their work, the thermo-mechanical TIG welding analysis was carried out utilizing a systematic process that was then verified by trials. Based on the research, a correct calibration of the heat source based on experimental measurements was added into the numerical model, overcoming the uncertainty of the results by correlating the final temperature distribution with the experimental observations. The process has minimal temperature fluctuation in the quasi-steady state condition, which can reach up to 1686C, according to measurements made using IR thermography and FEM at different timings. The welding line's heating and cooling rates, which are stable throughout the process and are observed at different points in the quasi-steady state condition, are 229.5C s1 and 85.8C s1, respectively. The experimental measurement, which has a reasonable level of precision, is consistent with the surface and nominal residual stress predictions. This thermo-mechanical study guarantees that the interpretation of surface and nominal residual stress data is more straightforward and accurate. The distortion forecast and the measurements from the experiments show a clear agreement. The experiment's unclamping phase, which was not included in the simulation, is what led to the tiny deviations. The capability of IR thermography to validate the temperature distribution predicted by FEM was demonstrated in their work. Additionally, utilizing FEM, surface and nominal residual stress profiles were accurately created and confirmed using non-destructive techniques.

Prashant Sagar, et al [6] studied the thermal analysis of TIG welded Ti-6Al-4V plates using ANSYS.They eventually came to the conclusion that the ANSYS model created in their study was in straight agreement with experimental data following TIG welding on Ti-6Al-4V at various welding rates. Due to the significant heat concentration at low speeds, it was discovered through the analysis of the ANSYS temperature profile that the heat impacted zone is more prevalent at lowspeed welding specimens and much less so at high speeds. Their research also found that as welding speed increases, temperature lowers.

Antony Solomon.S, et al [7] processed the simulation and modelling of the effect of welding process parameters of Inconel 625. In their work, the model was initially created in CAD software before being loaded into ANSYS. The material parameters of the Inconel 625 alloy were imported, and the predicted heat flow was provided as an input boundary condition with regard to the welding speed. It is possible to determine the length and distribution of temperature over the plate. Following that, the structural analysis is given the temperature distribution as input, and the neigh boring sides of the plate are also given fixed support. Calculated is the maximum tension placed on the weld center area. Each experimental trial receives the aforementioned analysis in accordance with the experimental design. Finally, all of the trail results are calculated and entered into the Design Expert software's Historical data design section under the Response Surface Methodology. The mathematical model needed for the analysis was discovered. It is verified by a parameter that is randomly chosen, and the actual and predicted values are compared using Ansys. The mathematical model is reliable because the divergence is within 10%. The maximum temperature was discovered through their research to be mostly dependent on welding current and stress created on the weld region to be dependent on welding speed.

Tauheed Shehbaza, et al [8] studied the dissimilar P-TIG Welding between Inconel 718 and commercially pure titanium using niobium interlayer. In their study, Nb was used as the interlayer in P-TIG-welded CpTi/IN718 joints, and after the joints were successfully produced and characterized, the melted region formed at the side of the CpTi that faced the arc showed a higher proportion of Nb dissolving due to the high arc temperature and thermal conductivity of the CpTi. Ni and Ti's reactivity was constrained by Nb, which also served as an effective interlayer to prevent the development of brittle Ni/Ti IMCs. The weldment's tensile strength was determined to be 150 Mpa. High residual stresses, the presence of fractures, and the development of brittle IMCs are all responsible for the decrease in strength. Due to Ti and Nb's mutual solubility, a solid solution formed, identifying the CpTi and Nb contact. Additionally, no IMCs developed at the CpTi/Nb interface. NbNi3, and Nb7Ni6 intermetallics were produced as a result of the eutectic reaction at the Nb/IN718 contact. In comparison to other areas of the weldment, the diffused layer that formed at the Nb/IN718 interface had the highest microhardness, measuring 782 HV. Additionally, because to the existence of the hard IMCs, a microhardness that was approximately 64% higher at the Nb/IN718 contact than the CpTi/Nb interface was noted. Similar to the Nb interlayer, the diffused layer had the highest

nanohardness (14.62 GPa), which was 10.3 and 3.7 times higher than the BM of the IN718 alloy.

Jing Liu, et al [9] conducted a study on microstructure and mechanical properties of laser welding of Ti6Al4V to Inconel 718 using Nb /Cu interlayer.They employed the laser welding induced brazing-welding approach to produce hybrids with the unmelted Nb separating the fusion zone from the brazing reaction zone. The brazing layer, which is composed primarily of solid solutions based on Nb, Cu, and Ni, formed between Nb and Inconel 718 as a result of the melting of Cu foil, and the fusion zone, which includes solutions based on Ti that were created at the Ti/Nb interface. The connection with the Nb/Cu multi-interlayer had the highest tensile strength, measuring 260 MPa, although it fractured in a brittle-like manner. Due to the immiscibility of Cu and Nb and the rapid heating and cooling rates of laser welding, voids formed at the Nb/Cu/Inconel718 interaction may assist prevent the development of IMCs and may be the cause of the joint's brittle fracture.

Timo Rautio, et al [10] studied the laser welding of selective laser melted Ti6Al4V. They conducted research on the microstructural evolution and tensile properties of Ti6Al4V produced through additive manufacturing at two different layer thicknesses of 30 and 50 mm and came to the conclusion that the layer thickness t has a significant impact on the microstructure that is formed. The primary phase structure of the material in its constructed state is acicular '-martensite, however following post-annealing at 940 C, the microstructure mostly comprises of coarse a platelets with inter-lamellar. With a yield strength of 910 MPa, ultimate tensile strength of 1080 MPa, and elongation to fracture of 15% at t = 30 mm, an excellent strength-ductility combination was achieved. The microstructures of the weld zone exhibit fine needle-shaped -martensite at multidirectional distribution in both the as-built and post-annealing states. The laser welded materials achieved a nearly 100% junction efficiency in terms of tensile strength. Additionally, there were no ductility losses in the laser welds.

Chao Chen, et al [11] investigated the and microstructure of Ti-6Al-4V weld bead during pulse ultrasound assisted TIG welding. When compared to TIG, the weld penetration and weld width of PU-TIG were increased by about 46% and 27%, respectively, when the

pulsed frequency was greater than 10 Hz in their study on the formation and microstructure of Ti-6Al-4V weld beads created during pulse ultrasound assisted TIG welding. As the ultrasonic power in the U-TIG grew, so did the weld breadth and weld penetration. The PU-TIG of 10 Hz had weld geometric parameters that were similar to the U-TIG of 2400 W. In comparison to the TIG, the grain sizes in the U-TIG and PU-TIG were smaller and the grain size distributions were more distributed. In the 10 Hz PU-TIG, the minimum grain diameter of 148 m was achieved, which was a reduction of around 0.5 times when compared to the TIG. The TIG weld seam had an average hardness of about 348 HV. The average toughness of the weld seam in a U-TIG was 370 HV when the ultrasonic power was 2.4 kW. The weld seam's average toughness in PU-TIG was about 370 HV.

C. Mukundhan, et al [12] conducted a study on microstructure and tensile properties of linear friction welded Ti-6Al-4V alloy joints. They conducted Ti-6Al-4V linear friction welding and came to the conclusion that an increase in FRNP from 15 MPa to 20 MPa indicated an improvement in the tensile characteristics of joints. It is primarily connected to achieving the ideal frictional heating, which leads to the refinement of grain structure at the joint contact. Additional increases in FRNP up to 25 MPa revealed a decrease in the tensile characteristics of joints. It is mostly associated with an increase in friction heat that causes grain coarsening in various LFW joint locations. The LF welded Ti6Al4V joints had better tensile strength (UTS) of 993 MPa and elongation (EL) of 8% when created with the recommended level of FRNP of 20 MPa. As a result, the FRNP level was examined for its use in the manufacturing of LFW using Ti6Al4V alloy. The joints' notch strength ratio (NSR) of 1.041 and notch tensile strength (NTS) of 1073 MPa indicated ductile fracture. The UTS, NTS, and EL of the parent metal were found in 96.41%, 104.10%, and 66.67% of the LF welded Ti6Al4V joints. The highest refinement of alpha + beta grains at the joint interface is mostly attributed to the higher smooth and notch tensile characteristics of joints. At the weld nugget zone, the bimodal α-β microstructure changed into Widmanstatten (α), martensite (α’), and β structure. Different areas of the weld cross-section have microhardness inhomogeneities. The weld center zone among these areas has a maximum hardness of 440 HV. Because of the coarsening of the grain and consequent weakening of LFW joints, most failures happened at the TMAZ.

Balrm Yelamasetti, et al [13] studied the metallurgical, mechanical and corrosion behaviour of pulsed and constant current TIG dissimilar welds of AISI 430 and Inconel 718. They investigated how different TIG welding current modes affected the microstructural characteristics, tensile strength, microhardness, and corrosion resistance behavior of weldments made of AISI 430 and Inconel and filled with ERNiCrMo-4. The key findings from their research include both of the successful welding techniques used to combine the dissimilar aforementioned plates employing ERNiCrMo-4 as filler. Additionally, the radiography results showed no macro or micro flaws in the weld structures of the two weldments. In PC-TIG weldments, grain expansion and cellular dendritic phase structures were seen, but in CC-TIG weldments, grain coarsening with Martensite phases were seen. Strong alloying elements like Nb and Mo ensure that there won't be any solidification cracking or HAZ liquid cracking in the PC-TIG weldment. Comparing PC-TIG weldment to CC-TIG weldment and base metal AISI 430, it was shown to have higher tensile characteristics. Additionally, a greater YS to UTS value ratio was seen in PC-TIG weldments. Due to the creation of skeletal delta ferrite morphology, the fusion zone and HAZ of PC-TIG weldments were harder than CC-TIG weldments. Contrary to CC-TIG weldment (1.41 mm/year), the corrosion rate of PC-TIG weldment was observed to be 1.35 mm/year. In comparison to CC-TIG welding and the base metal Inconel 718, PC-TIG welding demonstrated superior corrosion resistance behavior. Better mechanical qualities, superior corrosion resistance, and the development of fine grain structures, particularly at the roots, are all characteristics of weldments created by PC-TIG welding.

E. Ahmadi, et al [14] conducted a study on the mechanical response and wear behavior of graphene reinforced Inconel 718 composite produced via hybrid accumulative roll bonding and gas tungsten arc welding process. In their study, Inconel 718 reinforced with GNPs was created using a hybrid ARB-GTAW method, and evaluations of the composites' microstructure, phases, microhardness, wear, and mechanical characteristics were made. The key discovery from their research was that the composites reinforced with 1.0% GNP had an average microhardness that was 1.125 times higher than that of the IN718 alloy. Yield strength (1170 MPa), ultimate tensile strength (1400 MPa), and Vickers hardness (HV 600) all improve by 40%, 50%, and 35%, respectively, with the addition of 1.0% GNP to the matrix. When GNPs are added to the superalloy via the aforementioned method, both the friction coefficient and wear rate significantly reduce. For the Inconel 718 alloy with 1.0% GNPs as compared to

IN718 the average friction coefficient is reduced by 55% to a value of 0.36 and the wear rate is reduced by 65% to a value of 4.58× 10^-4mm3/Nm. The reinforcement mechanisms provided by GNPs and contemporaneous development of an anti-wear shielding film through the sliding contact surface are responsible for the improved tribological behavior of composite specimens. The GNP residues are still present in the composites, although some of it has been removed due to the hot weld pool. NbC carbides are created when unbound carbon and metal atoms combine. Low defect density in the graphene structure, as shown by Raman spectroscopy investigation, implies that the structural integrity of GNPs is maintained during the hybrid ARB-GTAW production method of composite.

Jacek Gorka, et al [15] studied the effect of TIG welding on the structure and hardness of butt joints made of Inconel 718. They investigated the impact of welding 1.0 mm thick sheets using the TIG method and came to the conclusion that increasing the welding linear energy within the adopted range increased the breadth of the weld and that of the HAZ. The joints created with the highest linear energy, or 80 J/mm, had the widest HAZ, weld face, and weld root dimensions. The austenitic matrix, which is characterized by a range of grain sizes and precipitate quantities, was present in the base material structure; grain sizes were constrained to be between 5 and 20 micrometers. Regardless of the welding parameters used, the structure of the weld included a zone of columnar grains oriented towards the fusion line, large groups of primary dendritic grains with clearly revealed primary axes of variously oriented dendrites, and precipitates in the form of low-melting eutectics in the interdendritic spaces. The dendritic axis areas were identified by the chemical composition related to the solution matrix, according to the microanalysis of the weld in the Inconel 718 joints. In turn, the makeup of individual precipitates in the interdendritic regions revealed the presence of carbides of the Nb(TiMo)C or Mo(Ni)6C type. The eutectic precipitates' chemical make-up suggested the presence of the Laves phase ((FeNiCr)2(NbMoTiSi)) and the intermetallic phases (Ni3(NbAlTi), Ni3(AlTi), and Ni3Nb). In the HAZ and BM of the welded joints, the microanalysis of individual precipitates of secondary phases revealed the presence of carbides primarily of the M23C6 type, such as Cr23C6, as well as carbides rich in niobium and titanium, most likely of the MC or M2C type, such as Nb(Ti)C or Nb(Ti)2C and Nb(TiB)C. The hardness values in the tested portions of the welded joints did not show a clear effect on the welding conditions that were used. The weld area's hardness was noticeably higher than the base material's and the HAZ's, which together made up the joints.

# CHAPTER 3
# SIMULATION THROUGH CATIA

## 3.1 METHODOLOGY

The research's methodology describes the materials and analysis methods utilized to examine the alloys chosen for welding as well as the welds produced by comparable and dissimilar alloys. Hardness, tensile and compressive strength, among other qualities, are taken in mind when analyzing the alloys. It gives details on the alloys that were utilized in the welding process. Utilizing CATIA V5, the geometries and attributes will be designed and assessed.

## 3.2. SCOPE OF APPLICATION OF CATIA SOFTWARE

- Mechanical Engineering.
- Design.
- System engineering.
- Fluid system.
- Electrical system.

## 3.3. STEP BY STEP PROCEDURE FOR THE SIMULATION.

1. Open CATIA.
2. Go to file in CATIA.
3. Click on new, select part.
4. Name the part which you are going to make.
5. Select x-y plane.
6. Select the sketch tool to create the profile of the object.
7. Select tool to create a rectangle.
8. Then sketch a rectangle of 100mm×60 mm.
9. Exit from the sketch tool by clicking on exit workbench.

10. Select the Pad tool to create the thickness of 2 mm.

11. Select object from the tree and apply the material.

12. Apply the mesh size.

13. Use the clamp command to fix the two end and then apply the load of 50 N and then click to compute.

14. Then click to different mechanical property for the analysis.

### 3.4. THREE DIMENSIONAL VIEW OF OBJECT.

The structural analysis for this work was done using CATIA software to ensure accuracy. The specimen size is obtained in accordance with the ASTM D 790 standard for the best results. For the purposes of analysis, deformation, von Mises, displacement, and primary stress have been determined here. The comparative study performed using the CATIA program is shown in Figs. 3.1-3.13.

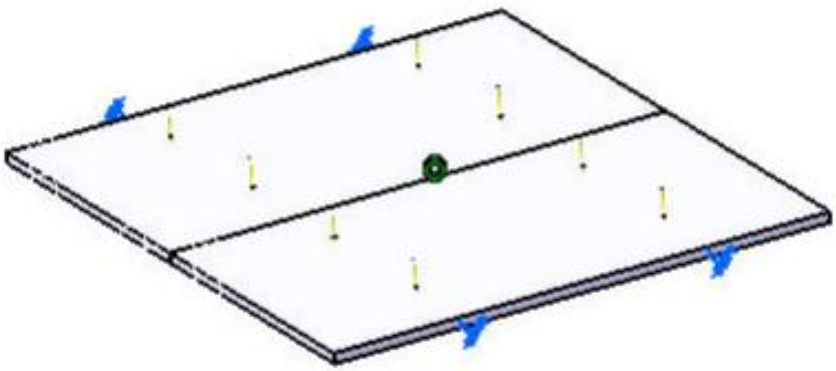

Fig 3.1: The geometry created in CATIA

### 3.5. FLEXURAL TEST

The flexural or bending test determines how much force is needed to bend the weld joint under three-point loading. The results of this test are used to calculate the load that the weld can withstand without bending. The flexural modulus of a material is used to mean how rigid it is when flexed. Since the physical properties of materials can vary depending on ambient temperature, testing materials at temperatures that simulate the intended end use environment is often necessary.

The input parametrs for the simulation approach is shown in Table 3.1.

Table 3.1: The input parameters for the simulation

| Parameters | Inconel 718 | Ti6Al4V |
|---|---|---|
| Young modulus | 9.399e+10N_m2 | 1.65e+011N_m2 |
| Poisson ratio | 0.3 | 0.27 |
| Density | 4368.1kg_m3 | 8219kg_m3 |
| Yield strength | 8.8e+008N_m2 | 1.1e+009N_m2 |
| Thermal expansion | 8.5e-006_Kdeg | 1.3e-005_Kdeg |

### 3.5.1 DEFORMATION IN THE WELD.

The magnitude of load on the each welded joints is 100 N inorder to find the variation in the deformation. When an object is subjected to a load of it can deform in size or shape.

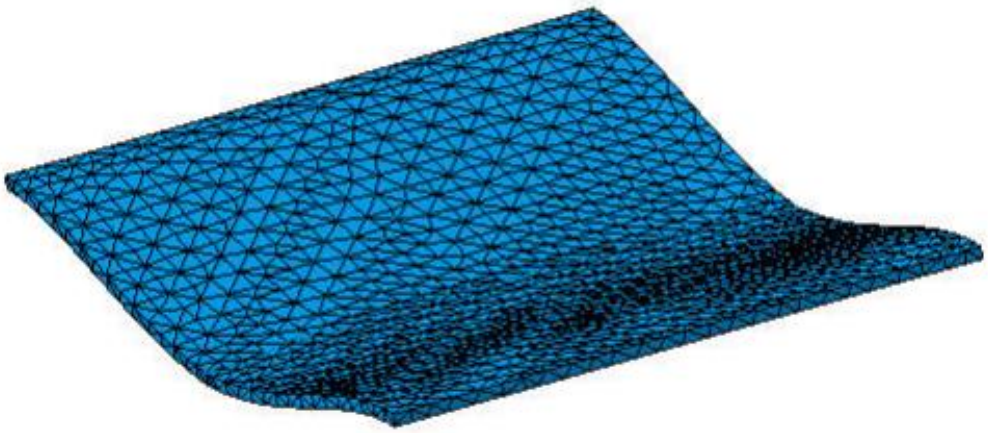

Fig 3.2: Deformed mesh in similar welded region of Inconel 718

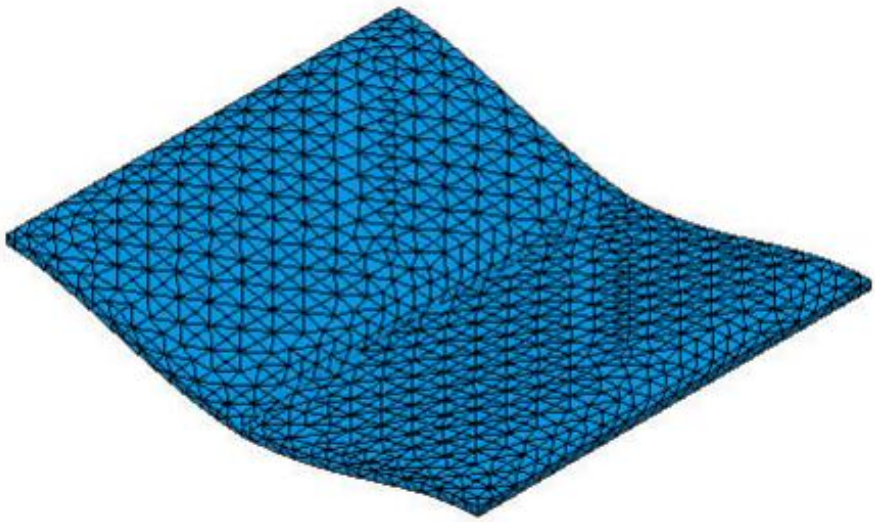

Fig 3.3: Deformed mesh in similar welded region of Ti6Al4

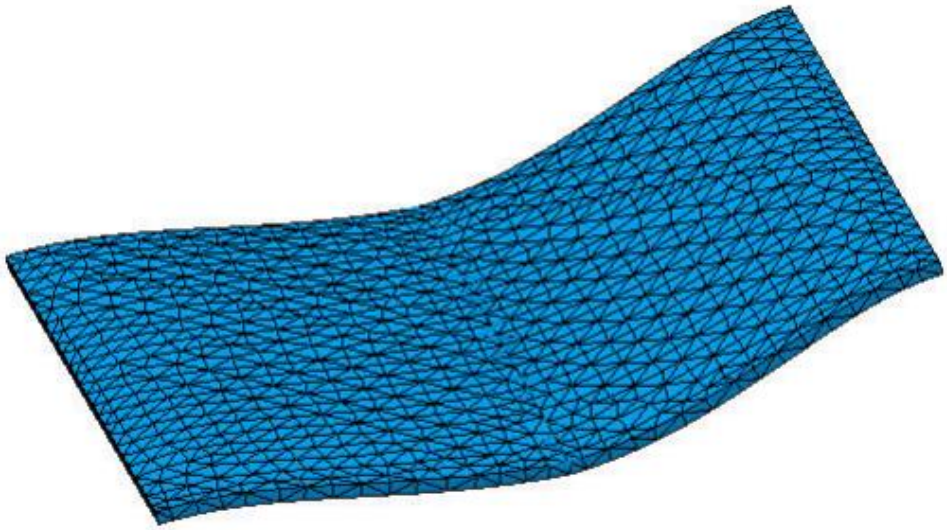

Fig 3.4: Deformation in the dissimilar welded region of Inconel 718 with Ti6Al4V

### 3.5.2 VON MISES STRESS DISTRIBUTION IN THE WELD.

The Von Mises stress values assist us in deciding whether a given weld can yield or fracture under the load. According to the von Mises yield criterion, if a substantial's von Mises stress is equal to or greater than the yield limit of the weld under simple strain, the weld will yield as shown in Figs 3.5-3.7 and the associated values of von mises stress shown in Table 3.1.

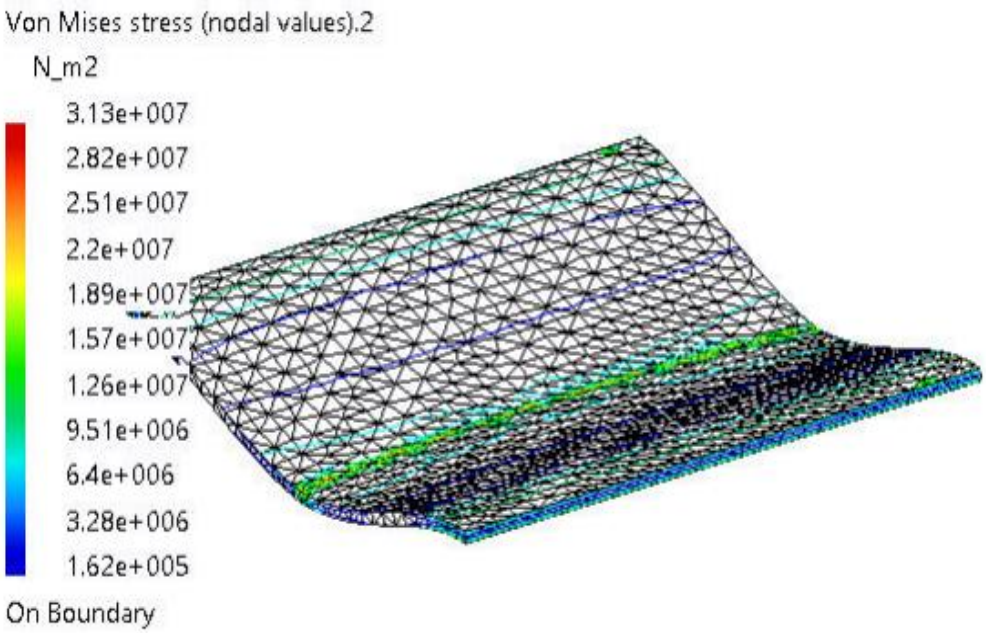


Fig 3.5: The Von Mises stress distribution in similar welded region of Inconel 718

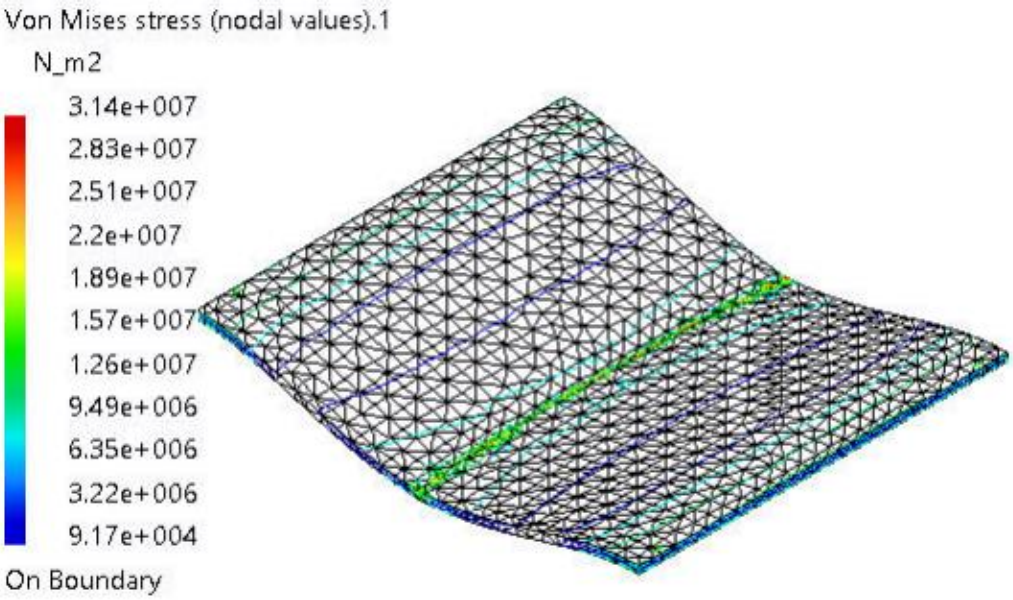


Fig 3.6: The Von Mises stress distribution in similar welded region of Ti6Al4V

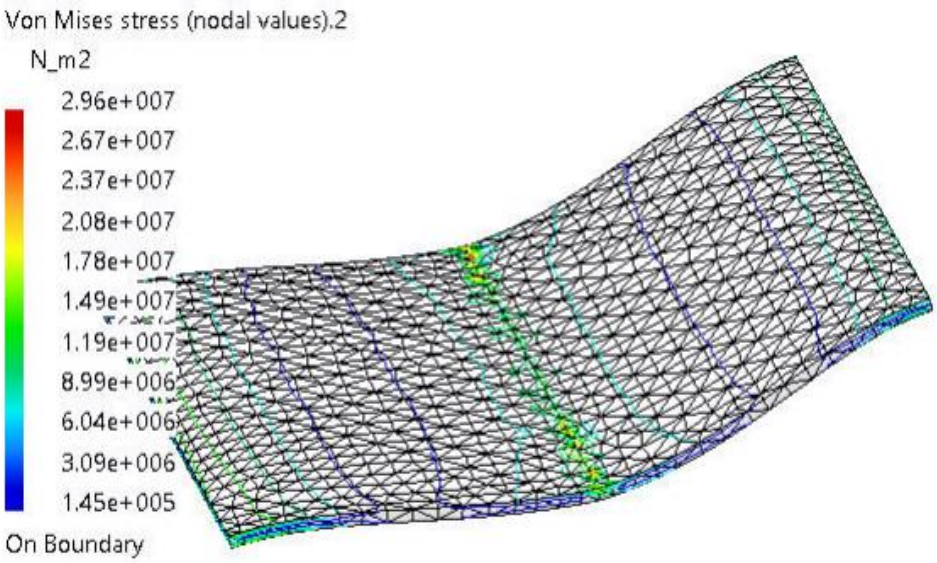


Fig 3.7: The Von Mises stress distribution in dissimilar welded region of Inconel 718 with Ti6Al4V

Table 3.2: The Von Mises stress distribution of different welds

| Weld Produced | Minimum [ $Nm^{-2}$ ] | Maximum[$Nm^{-2}$ ] | Average [ $Nm^{-2}$ ] |
|---|---|---|---|
| In718 – In718 | 1381.75778 | 3836.607826 | 1227.425023 |
| Ti6Al4V- Ti6Al4V | 1381.75778 | 3828.53925 | 1223.390735 |
| In718- Ti6Al4V | 1304.993459 | 3626.824853 | 1160.915697 |

### 3.5.3 DISPLACEMENT IN THE WELD

In mechanics, displacement is the distance travelled by a particle or body in a particular direction under the influence of a load as shown in Figs 3.8-3.10 and the associated values of displacement shown in Table 3.2.

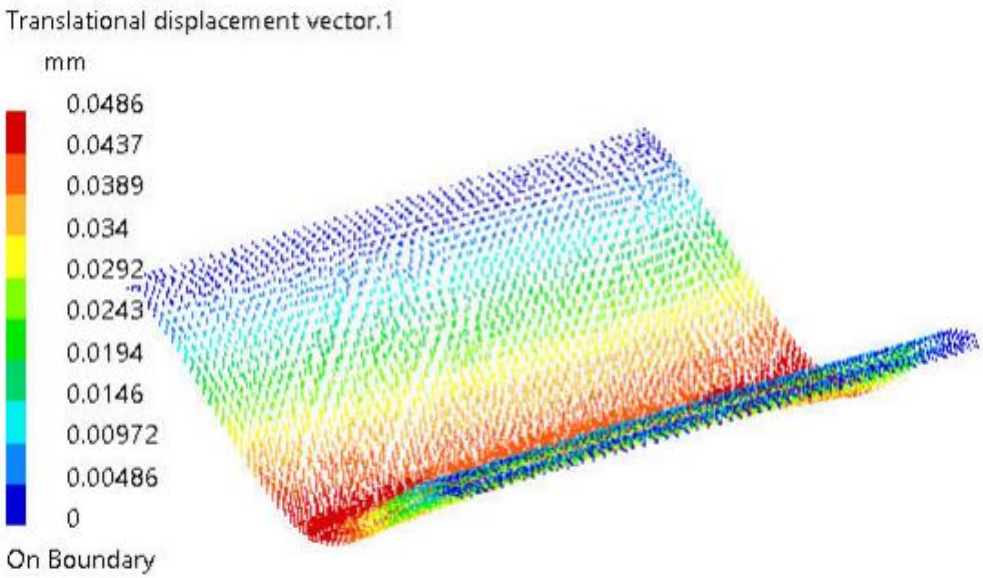


Fig 3.8: The translational displacement in similar welded region of Inconel 718

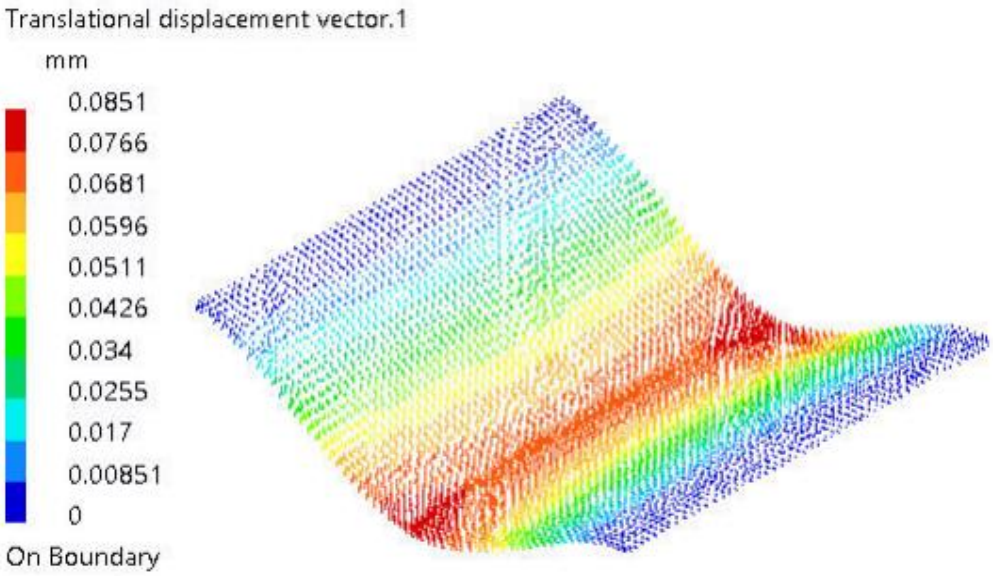


Fig 3.9: The translational displacement in similar welded region of Ti6Al4V

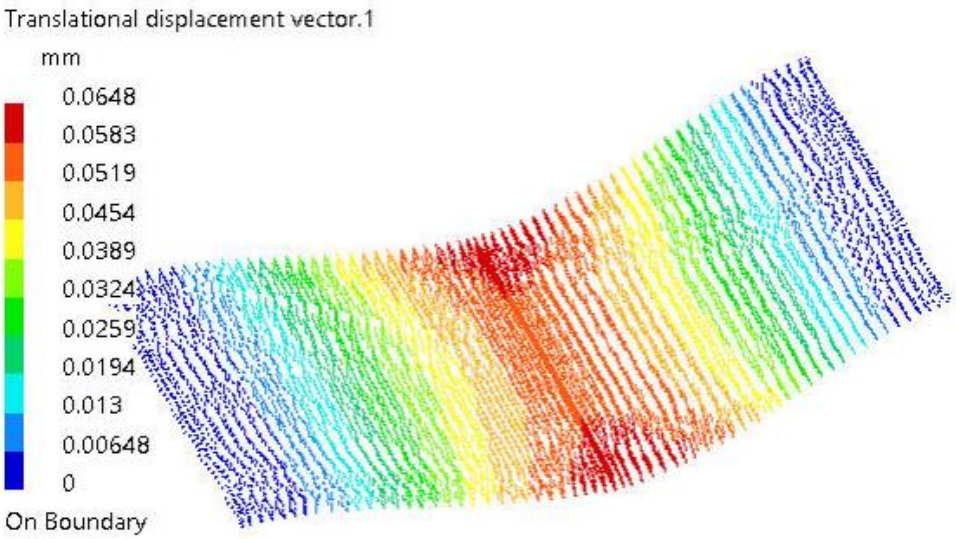


Fig 3.10: The translational displacement in dissimilar welded region of Inconel 718 with Ti6Al4V

Table 3.3: The magnitude of translational displacement of different welds

| Weld Produced | Minimum [ $Nm^{-2}$ ] | Maximum[$Nm^{-2}$ ] | Average [ $Nm^{-2}$ ] |
|---|---|---|---|
| In718 – In718 | 0 | 0.0486 | 0.0243 |
| Ti6Al4V- Ti6Al4V | 0 | 0.0851 | 0.04255 |
| In718- Ti6Al4V | 0 | 0.0648 | 0.0324 |

### 3.5.4 PRINCIPAL STRESS IN DISTRIBUTION IN THE WELD.

Principal stresses are the maximum and minimum (extremum) extensional (normal) stresses in a stress state at a point. The principal directions have no shear stresses associated with them as shown in Figs 3.11-3.13 and the associated values of principal shown in Table 3.3.

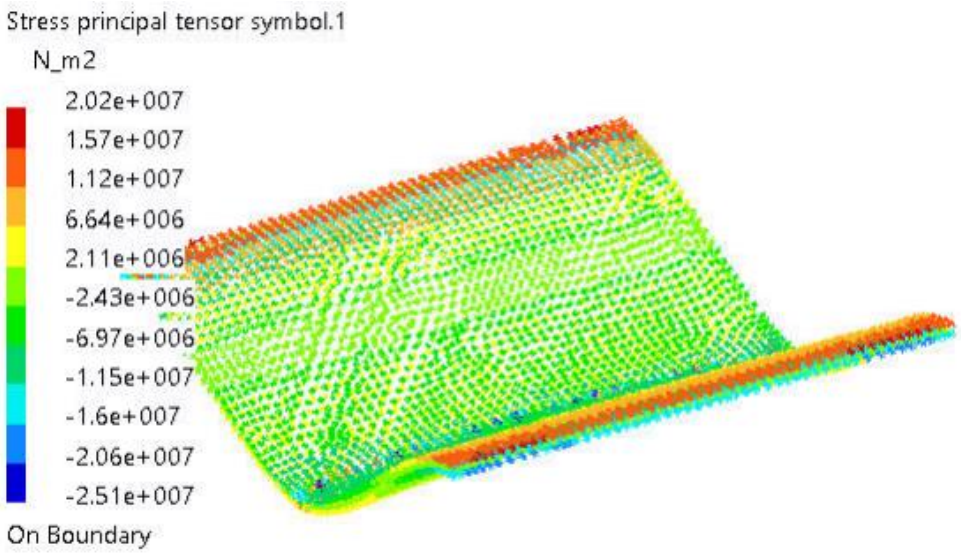


Fig 3.11: The Principal Stress in similar welded region of Inconel 718

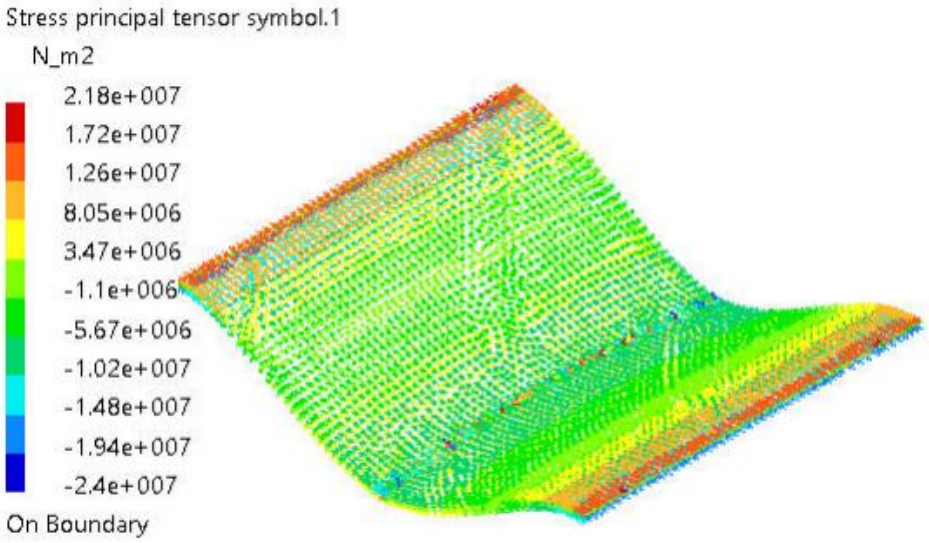


Fig 3.12: The Principal Stress in similar welded region of Ti6Al4V

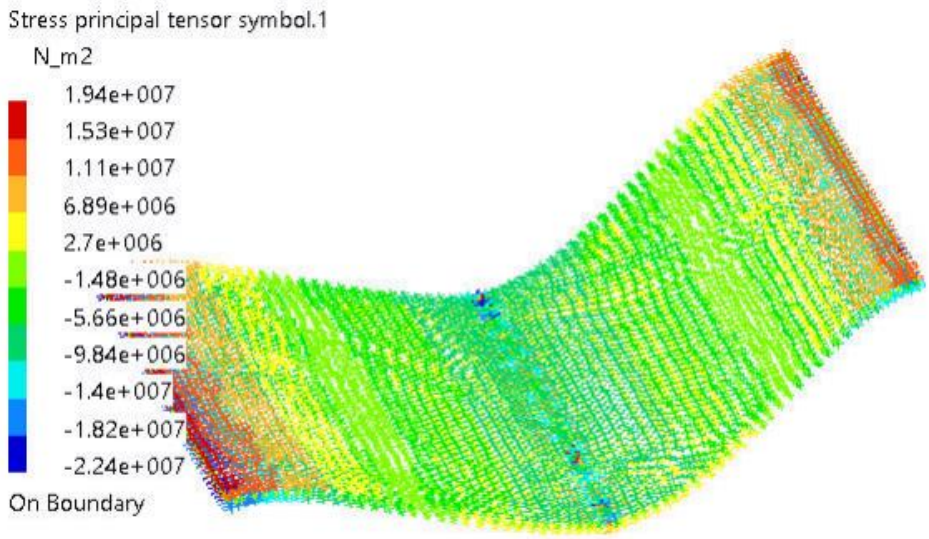


Fig 3.13: The Principal Stress in dissimilar welded region of Inconel 718 with Ti6Al4V

Table 3.4: The magnitude of principal stresses of different welds

| Weld Produced | Minimum [ $Nm^{-2}$ ] | Maximum[$Nm^{-2}$ ] | Average [ $Nm^{-2}$ ] |
|---|---|---|---|
| In718 – In718 | -2811.898691 | 2678.767189 | 5490.66588 |
| Ti6Al4V- Ti6Al4V | -2287.441259 | 3247.601788 | 2767.521524 |
| In718- Ti6Al4V | -3969.739328 | 2779.624387 | 6749.363715 |

# CHAPTER 4

# EXPERIMENTAL SETUP AND PROCEDURE

## 4.1 SAMPLE PREPARATION

Wire-cut electrical discharge machining (WEDM) was used to cut the Inconel 718 and Ti6Al4V plates into coupons of 100 mm x 60 mm x 2 mm dimensions. Fig 1 represents the WEDM machine used for the sample preparation. Using dry spectroscopic techniques, the chemical composition of the plates was determined and is shown in Table. It was discovered that Inconel 718 and Ti6Al4V have respective ultimate tensile strengths of 1170 MPa and 1375 MPa. Thoroughly clean the sample before executing the wire cut EDM procedure to get rid of any contaminants, like dirt, grease, corrosion, or oxide coatings. The success of the EDM process depends on this stage.


Fig 4.1: WEDM Machine

Table 4.1: Chemical composition (wt%) of Ti6Al4V and Inconel 718

| | Ti | Inconel 718 |
|---|---|---|
| Ti | Balance | 0.7-1.15 |
| Al | 5.5-6.8 | 0.2-0.8 |
| V | 3.5-4.5 | - |
| Fe | <0.3 | Balance |
| Cr | - | 17-21 |
| Nb | - | 4.75-5.5 |
| Mo | - | 2.8-3.3 |
| Ni | - | 50-55 |

## 4.2 WELDING OF INCONEL 718


Fig 4.2: TIG welding machine


Fig 4.3: The weld joint formed between the Inconel 718 plate

The base metal sheets were cleaned mechanically and chemically to get rid of moisture, grease, corrosion, scale, and other impurities before welding. Using a fixture and mechanical clamp. For this experiment, a manual-mode automatic TIG welding equipment was used. The temperature has not been kept at a free heat level. The shielding gas used in welding had a 15L/min flow rate. A tungsten electrode with a 2mm throat was used for the welding. A single pass of welding was used to achieve complete penetration. Since manual mode TIG welding was employed for the experiment, the welding speed was estimated with extreme care. The mechanical properties and parameters used for the welding operation is mentioned in table 4.2 and table 4.3 respectively.

Table 4.2: The mechanical properties of Inconel 718

| | |
|---|---|
| UTS (MPa) | 1034 |
| YS (MPa) | 829 |
| % Elongation | 20 |
| Hardness | 40RC |

Table 4.3: The welding parameters

| | |
|---|---|
| Current (Amp) | 50 |
| Voltage (Volt) | 12 |
| Speed (mm/sec) | .8 |
| Heat Input (KJ/mm) | .5 |

As-welded Inconel 718 was found to have micro-hardness, residual stress, and tensile strength of 226 HV, 48 MPa, and 885 MPa, respectively [2].

## 4.3 WELDING OF Ti6Al4V


Fig 4.4: The weld joint formed between Ti6Al4V

The same procedures used for the Inconel 718 have been repeated for the welding operation, The mechanical properties and parameters used for the welding operation is mentioned in table 4.4, table respectively.

Table 4.4: The mechanical properties of Ti6Al4V

| | |
|---|---|
| UTS (MPa) | 950 |
| YS (MPa) | 880 |
| % Elongation | 14 |
| Hardness | 34RC |

The as-welded Ti6Al4V was found to have micro-hardness, residual stress, and tensile strengths of 327.4 ± 6.1 HV, 50 ± 16.2 MPa, and 850 ± 14.2 MPa, respectively [3].

## 4.4 WELDING OF INCONEL 718 WITH Ti6Al4V

The tig welding of Inconel 718 and Ti6Al4V was carried out at the welding parameters of welding voltage 12V, welding current 50A and the flow rate of 15L/min. Fig represents the tig welding machine used for the welding operation. Fig shows the generated weld between the Inconel 718 and Ti6Al4V plates.

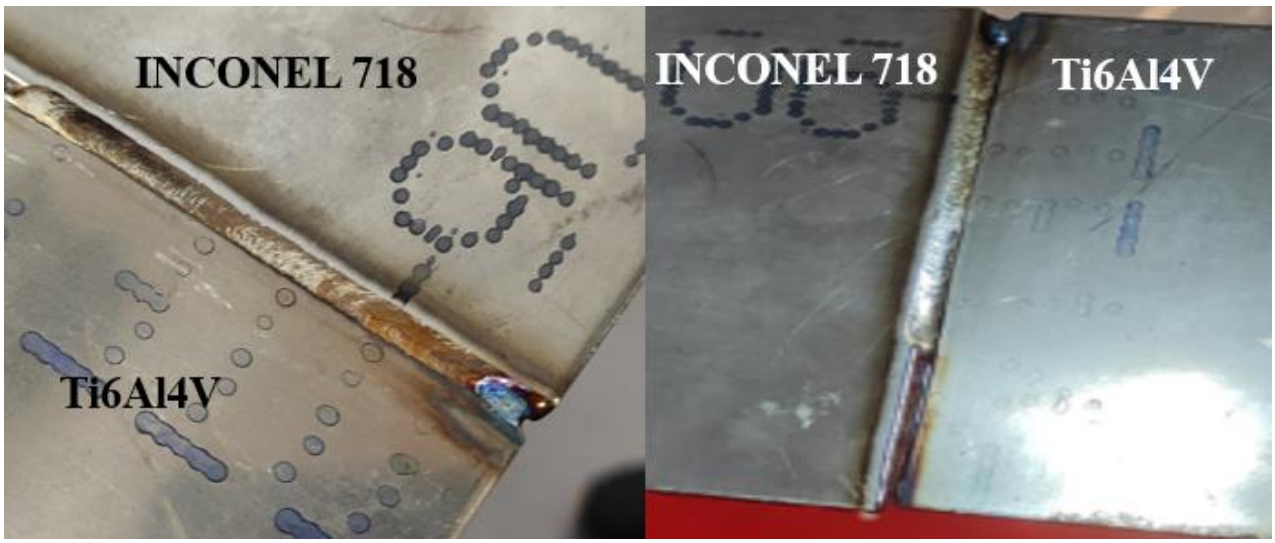


Fig 4.5: The weld generated

## 4.5 WELDING OF INCONEL 718 WITH Ti6Al4V IN THE PRESENCE OF $SiO_2$ FLUX POWDER

TIG welding was carried out using SiO2 flux powder. Before carrying out welding, the flux powder was uniformly mixed with the carrier solvent carbinol to obtain a paint-like consistency. This was manually applied using a paint brush to obtain a sufficiently layer thick [Fig 4.6]. Bead on trials were carried out on the plates using this flux. The welding operation was carried out at the welding parameters of welding voltage 12V, welding current 50A and the flow rate of 15L/min.

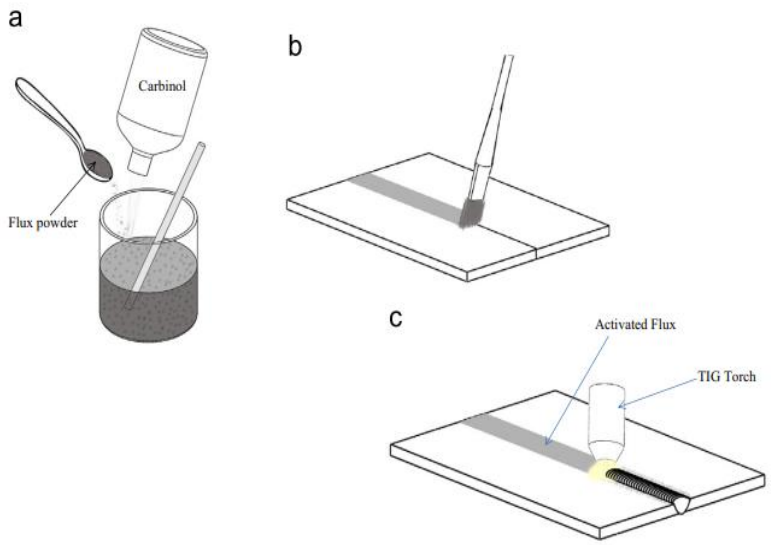


Fig 4.6: The schematic representation of applying flux powder [2]


Fig 4.7: The weld generated in the presence of SiO2 flux powder

## 4. 6 WELDING OF INCONEL 718 WITH Ti6Al4V WITH THE INSERTION OF NIOBIUM INTERLAYER

Due to the different physical and chemical properties of the two materials, straight joining of Ti6Al4Vand Inconel 718 is extremely difficult. Niobium was identified as a potential diffusion barrier between nickel and titanium because of its high melting temperature. The same welding conditions were employed for this welding operation, but an interlayer of 1.2mm Niobium was used between Inconel 718 and Ti6Al4V plates.

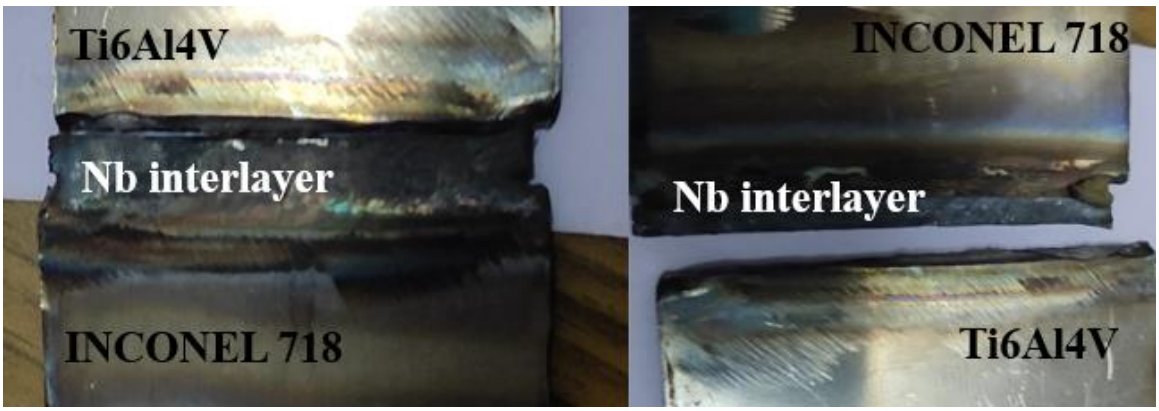


Fig 4.8: The weld generated with the insertion of niobium interlayer

# CHAPTER 5
# XRD ANALYSIS

X-ray diffraction (XRD) analysis is a technique used to determine the atomic or molecular structure of a crystalline material. It is based on the principle that when a beam of X-rays strikes a crystal, the X-rays are diffracted by the crystal lattice, producing a unique pattern of constructive and destructive interference. By analyzing the resulting diffraction pattern, valuable information about the crystal structure, lattice parameters, and other properties of the material can be obtained.

The theory of XRD analysis is rooted in Bragg's law, which relates the angles of incidence and diffraction of X-rays to the spacing between atomic planes in a crystal lattice. Bragg's law can be stated as follows:

$$n\lambda = 2d \sin(\theta)$$

Where:

n is an integer representing the order of diffraction.

$\lambda$ is the wavelength of the X-rays.

d is the spacing between atomic planes in the crystal lattice.

$\theta$ is the angle between the incident X-ray beam and the atomic planes.

According to Bragg's law, the X-rays will be diffracted at specific angles that depend on the lattice spacing of the crystal. By measuring the angles at which the X-rays are diffracted and knowing the X-ray wavelength, it is possible to determine the interplanar spacing in the crystal lattice.

In XRD analysis, a powdered sample or a single crystal is typically exposed to a beam of X-rays, and a detector records the intensities of the diffracted X-rays at different angles. The

resulting diffraction pattern is known as the X-ray powder diffraction pattern or the X-ray diffraction (XRD) pattern. This pattern contains a series of peaks corresponding to the different planes of atoms within the crystal lattice.

The positions and intensities of these diffraction peaks provide valuable information about the crystal structure, such as the lattice parameters, the orientation and size of the unit cell, the presence of impurities, and the arrangement of atoms within the crystal. XRD analysis can be used to identify unknown crystalline materials, determine the phase composition of a sample, investigate crystal defects, and study various physical and chemical properties of materials.

To extract information from an XRD pattern, various mathematical and computational techniques are employed, including peak fitting, indexing, and crystal structure refinement methods. These techniques allow researchers to interpret the diffraction data and derive quantitative information about the crystal structure and properties.

## 5.1: DIFFRACTION PEAK ANALYSIS

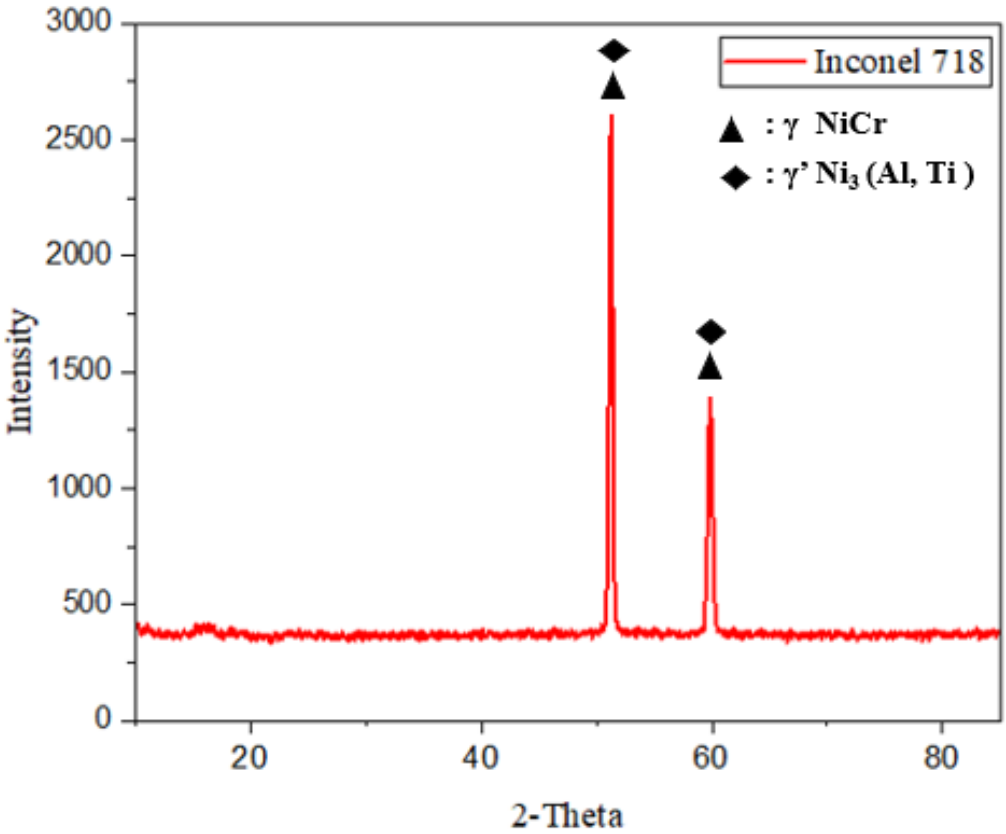


Fig 5.1 XRD diffraction peak of Inconel 718

γNiCrFe and γ' Ni3(Al, Ti) were proven to be present by the XRD diffraction peak of Inconel 718. The alloy with the chemical formula γNiCrFe, which contains the elements nickel (Ni), chromium (Cr), and iron (Fe), is present as gamma phase in Inconel 718. γNiCrFe alloys have a good corrosion resistance. This characteristic results from the alloy's surface developing a passive oxide layer that serves as a barrier against various corrosive environments, such as moisture, chemicals, and air conditions. γNiCrFe alloys are suitable for structural applications due to their high mechanical strength. These materials can sustain huge loads and mechanical stress thanks to their strong tensile strength, yield strength, and impact resistance. γNiCrFe alloys are appropriate for applications involving exposure to high heat because they can preserve their mechanical qualities at increased temperatures. They have a high melting point and maintain their stability and strength even when exposed to heat for an extended period of

time. In comparison to some other materials, γNiCrFe alloys have a comparatively low coefficient of thermal expansion, which means they expand or contract less with temperature changes. In applications where dimensional stability is crucial, this characteristic may be significant.

The superalloy composed of nickel (Ni), aluminum (Al), and titanium (Ti) has the element $\gamma Ni_3(Al, Ti)$ present in its gamma prime (γ') phase. These phases are well known for having outstanding mechanical qualities at high temperatures. Even at high temperatures, the alloy exhibits great strength thanks to the existence of the $\gamma Ni_3(Al, Ti)$ phase. For applications like gas turbines and jet engines, where the material must bear mechanical stress and creep at high temperatures, this feature is essential. Because of the $\gamma Ni_3(Al, Ti)$ phase's existence, materials can maintain their mechanical properties even after being exposed to high temperatures for an extended period of time. Materials used in high-temperature situations, where dimensional stability and structural integrity are crucial, must have this feature. The $\gamma Ni_3(Al, Ti)$ phase helps nickel-based superalloys have a reasonably high melting point, together with the other components. This characteristic enables these alloys to maintain their stability and strength at high temperatures, where other materials could weaken or disintegrate.

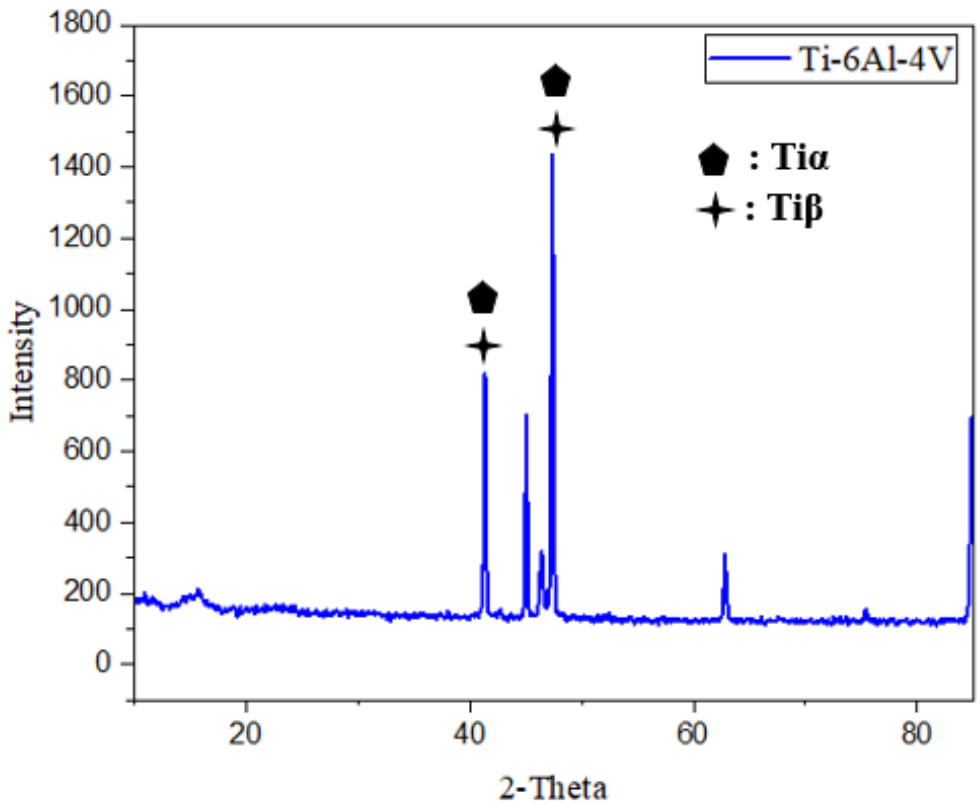

Fig 5.2: XRD diffraction peak of Ti6Al4V

The XRD diffraction peak determines the presence of Tiα and Tiβ elements in Ti6Al4V alloy. The term "Tiα" refers to the alpha (α) phase of titanium (Ti) which is a versatile metallic element known for its excellent strength-to-weight ratio, corrosion resistance, and biocompatibility. The properties of the Tiα phase exhibits good mechanical strength, making titanium alloys suitable for various structural applications. They possess a high tensile strength, allowing them to withstand heavy loads and mechanical stress. Tiα phase have a low density, about half that of steel. This lightweight property makes titanium attractive for applications where weight reduction is critical, such as aerospace, automotive, and sporting goods industries. The term "Tiβ" refers to the beta (β) phase of titanium (Ti) which is known for its excellent strength-to-weight ratio, corrosion resistance, and biocompatibility. The properties of the Tiβ phase exhibits high strength, making titanium alloys with this phase suitable for various structural applications. They possess a high tensile strength, allowing them to withstand heavy loads and mechanical stress. The Tiβ phase of titanium alloys exhibits good strength retention at elevated temperatures. This property makes them suitable for applications where high-temperature strength is required, such as in gas turbines and components for high-temperature environments.

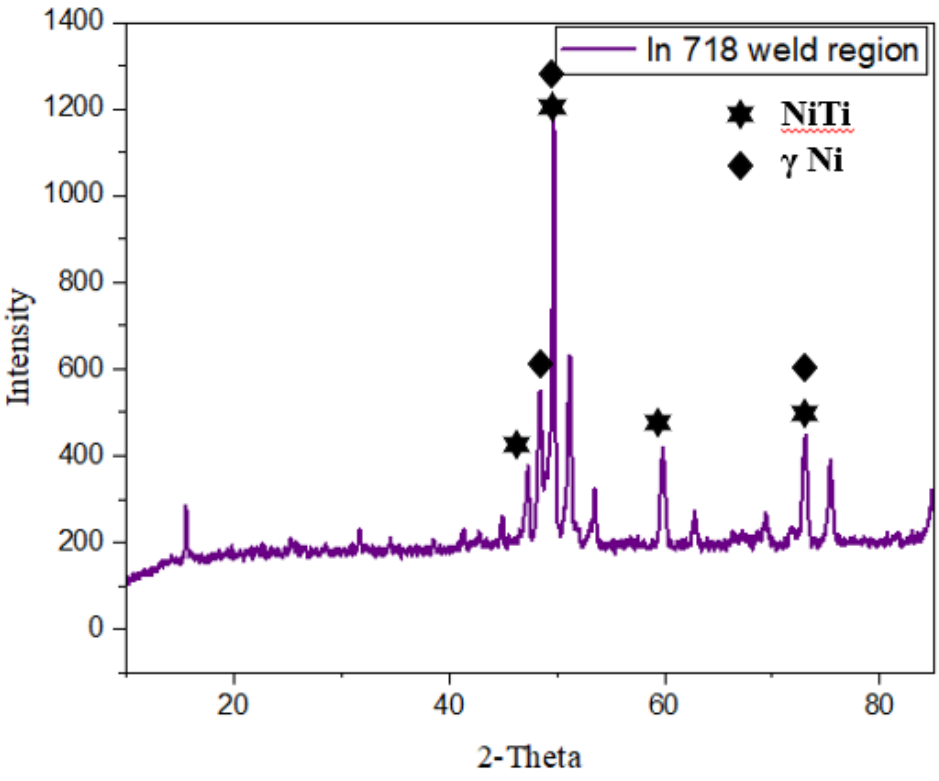

Fig 5.3: XRD diffraction peak of Inconel 718 weld region with Ti6Al4V

The diffraction peak of Inconel 718 weld region with Ti6Al4V proven the presence of NiTi and γNi compounds. NiTi is a unique element with a specific nature arising from its composition and phase transformation behavior. The brittle property of NiTi is a result of the reversible phase transformation between the austenite and martensite phases. NiTi exhibits a solid-state phase transformation between the high-temperature austenite phase and the low-temperature martensite phase. This transformation occurs due to the rearrangement of atoms within the material's crystal structure. The transition between these phases results in significant changes in mechanical properties and superelasticity. In the martensitic phase, NiTi exhibits a characteristic stress-induced martensitic transformation, enabling it to undergo significant strain without permanent deformation. Superelasticity is a desirable property in applications requiring flexibility, such as in medical devices and mechanical springs. Gamma nickel (γNi) refers to the face-centered cubic (FCC) phase of pure nickel. The key properties of γNi has a relatively high melting point which allows it to retain its structural integrity at high temperatures. γNi exhibits good ductility, allowing it to undergo plastic deformation without fracturing. This property makes it suitable for various forming and shaping processes. γNi has a relatively moderate coefficient of thermal expansion. This property is important in applications where dimensional stability is critical, as it allows for a balanced response to temperature changes and minimizes thermal stress.

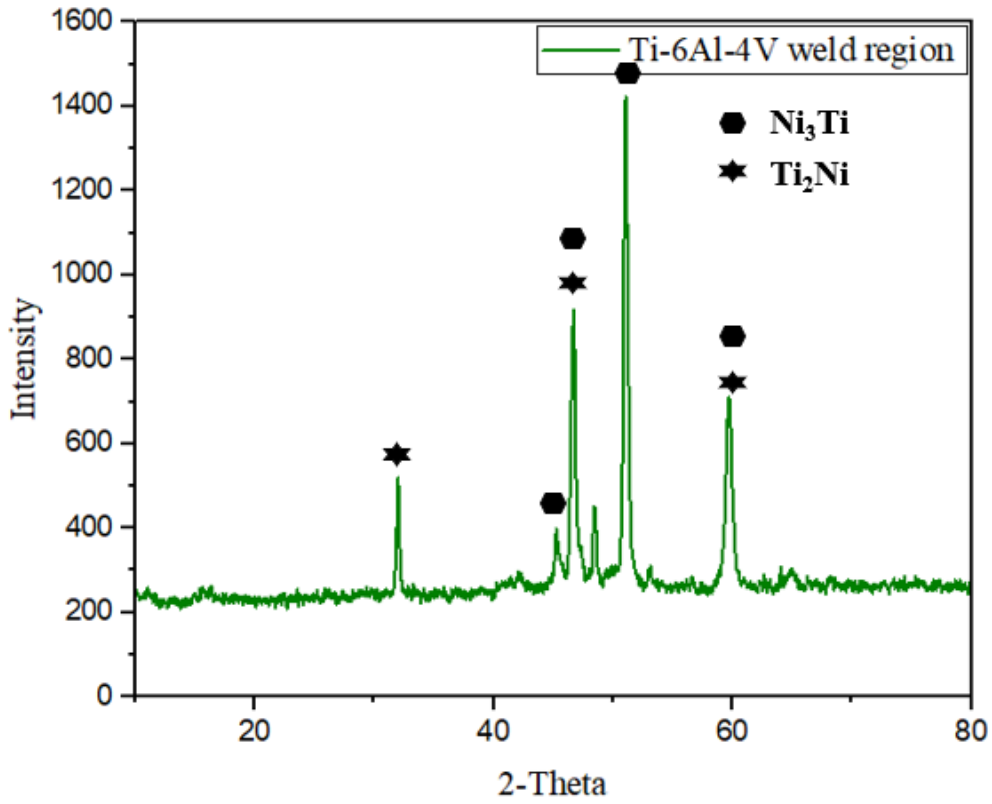


Fig 5.4: XRD diffraction peak of Ti6Al4V weld region with Inconel 718

The diffraction peak of Ti6Al4V weld region with In718 proven the presence of $Ni_3Ti$ and $Ti_2Ni$ compounds. The compound $Ni_3Ti$ refers to an intermetallic compound formed by combining nickel (Ni) and titanium (Ti). The crystal nature of $Ni_3Ti$ is known as the L12 structure. It belongs to the cubic crystal system and has a face-centered cubic (FCC) arrangement. The L12 structure is characterized by a specific arrangement of Ni and Ti atoms within the crystal lattice. $Ni_3Ti$ is an intermetallic compound, which means it forms a distinct phase separate from the pure metals. Intermetallic compounds often exhibit unique properties compared to the individual constituent metals. $Ni_3Ti$ can undergo a martensitic phase transformation. The transformation is typically between a high-temperature parent phase (austenite) and a low-temperature phase (martensite). The transformation involves a rearrangement of atoms within the crystal structure, resulting in changes in mechanical properties and shape. The compound $Ti_2Ni$ also refers to an intermetallic compound formed by combining titanium (Ti) and nickel (Ni). The crystal nature of has a specific crystal structure known as the Laves phase structure. It belongs to the hexagonal crystal system and has a close-packed hexagonal (CPH) arrangement. The Laves phase structure is characterized by alternating hexagonal and cubic layers of atoms within the crystal lattice. $Ti_2Ni$ is an

intermetallic compound, meaning it forms a distinct phase separate from the pure metals. $Ti_2Ni$ can display brittle behavior. Intermetallic compounds like $Ti_2Ni$ often exhibit a combination of brittle and ductile characteristics, depending on factors such as composition, microstructure, and testing conditions.

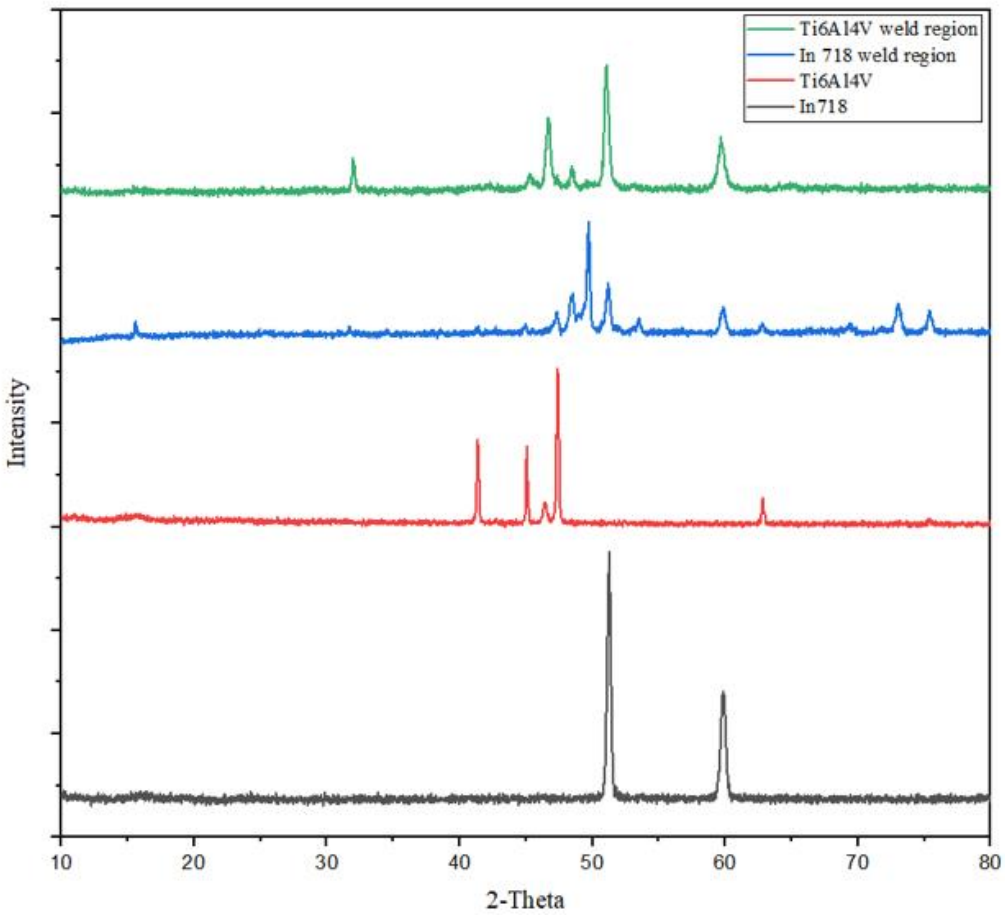


Fig 5.5: Combined XRD diffraction peak

The combined XRD diffraction peaks clearly describe the change in the atomic or molecular structure of the alloys. While considering the Inconel 718 alloy before and after welding operations, there is the formation of more peaks and intermetallic compounds such as NiTi and Ni. After the welding operation is conducted, the peaks in the Ti6Al4V region have been dismissed, and the formation of new peaks in the In718 alloy clearly explains the shifting of peaks. While in the case of the welded region of Ti6Al4V, more brittle intermetallic

compounds such as $Ni_3Ti$ and $Ti_2Ni$ have formed, which can be considered for the brittle nature of the weld region leading to the weld breakage.

## 5.2: INTERPRETATION OF XRD DATA

### 5.2.1. CRYSTALLITE SIZE DETECTION

Crystallite size determination in X-ray diffraction (XRD) analysis is a technique used to estimate the average size of the crystal domains (crystallites) present in a material based on the broadening of the XRD peaks. The Scherrer equation is commonly employed to calculate the crystallite size using the peak broadening information.

Here's an overview of the process:

Peak Broadening: When X-rays interact with a crystalline material, they are diffracted by the crystal lattice planes. The resulting diffraction pattern consists of sharp peaks that are subject to broadening due to several factors, including instrumental effects, strain, and finite crystallite size. The peak broadening primarily arises from the finite size of the crystallites.

Scherrer Equation: The Scherrer equation provides an estimate of the average crystallite size based on the peak broadening observed in the XRD pattern. The equation is as follows:

$$D = K\lambda / (\beta \cos \theta) ,$$

Where: D is the average crystallite size.

K is the Scherrer constant, typically taken as 0.9.

$\lambda$ is the wavelength of the X-ray used.

$\beta$ is the full width at half maximum (FWHM) of the diffraction peak after instrumental broadening corrections.

$\theta$ is the Bragg angle at which the diffraction peak occurs.

FWHM Determination: The FWHM value is obtained by analyzing the diffraction peak and measuring the angular width at half of the maximum peak intensity. It is crucial to correct for

instrumental broadening by subtracting the instrumental broadening contribution from the measured FWHM.

Calculation of Crystallite Size: Substituting the corrected FWHM value into the Scherrer equation allows for the calculation of the average crystallite size. It is important to note that this method provides an average value, assuming the crystallites are approximately spherical and randomly oriented.

Limitations and Considerations: The Scherrer equation provides an estimation of the average crystallite size, but it does not provide information about the size distribution or shape of the crystallites. Additionally, the calculated size can be influenced by factors like instrumental resolution, strain, and stacking faults. The technique is most applicable when the peak broadening is primarily due to crystallite size effects.

Crystallite size determination using XRD is widely utilized in materials science and characterization to assess the nanoscale structure of materials, including metals, alloys, ceramics, and thin films. Careful sample preparation, precise peak analysis, and consideration of the limitations are crucial for accurate and reliable crystallite size determination using XRD. Tables shows the average crystallite size obtained at different conditions.

Table 5.1: Crystallite size D (nm) of Inconel 718

| Peak position(2θ) | FWHM | Crystallite size D (nm) |
|---|---|---|
| 51.24413 | 0.35782 | 24.62321183 |
| 57.15625 | 0.38563 | 23.45890664 |

The average crystallite size of Inconel 718 = 24.04105924 nm

Table 5.2: Crystallite size D (nm) of Ti6Al4V

| Peak position(2θ) | FWHM | Crystallite size D (nm) |
|---|---|---|
| 41.36587 | 0.23304 | 31.8927 |
| 45.0631 | 0.2118 | 34.64538 |
| 46.42215 | 0.37364 | 19.54093 |
| 47.38623 | 0.24352 | 29.873 |
| 48.65066 | 0.01278 | 32.21566 |

The average crystallite size of Ti6Al4V = 29.63353 nm

Table 5.3: Crystallite size D (nm) of In718 weld region

| Peak position (2 θ) | FWHM | Crystallite size D (nm) |
|---|---|---|
| 49.70481 | 0.30132 | 23.92338984 |
| 51.17163 | 0.46107 | 15.54052062 |
| 53.47918 | 0.45512 | 15.58870706 |
| 48.7254 | 1.37698 | 5.255609492 |
| 47.24334 | 0.41861 | 17.38765663 |
| 15.5853 | 0.14342 | 54.88024981 |
| 59.82641 | 0.48297 | 14.25754279 |
| 62.78472 | 0.40133 | 16.89733156 |
| 69.34073 | 0.8508 | 7.679464239 |
| 73.02971 | 0.5194 | 12.29273364 |
| 75.40586 | 0.51815 | 12.1305799 |

The average crystallite size of Ti6Al4V = 17.80307 nm

Table 5.4: Crystallite size D (nm) of Ti6Al4V weld region

| Peak osition (2θ) | FWHM | crystallite size D (nm) |
|---|---|---|
| 46.36203 | 0.47349 | 15.42359 |
| 46.45807 | 0.48299 | 15.11478 |
| 46.67416 | 0.44399 | 16.42913 |
| 48.4594 | 0.32124 | 22.55154 |
| 51.06543 | 0.42214 | 16.9812 |
| 59.71168 | 0.63878 | 10.78607 |

The average crystallite size of Ti6Al4V = 16.21439 nm

### 5.2.2. LINEAR FIT, LATTICE STRAIN, AND CRYSTAL SIZE DETECTION

Linear fit, lattice structure, and crystal size are distinct aspects of XRD analysis. Here's a breakdown of each concept and how they relate to XRD:

Linear Fit: A linear fit in XRD refers to the process of fitting a straight line to a linear region of the diffraction pattern. This linear fit is typically performed to determine and subtract the background or baseline contribution from the XRD data. By subtracting the linear fit, the diffraction peaks become more prominent and easier to analyze. Figures and tables shows the linear fit data and graph at different conditions.

Lattice Strain: Lattice strain refers to the deformation or distortion of the crystal lattice from its ideal state. It can arise due to various factors, such as impurities, defects, and applied stress. Lattice strain affects the positions and shapes of the diffraction peaks in the XRD pattern. By

analyzing the peak positions, changes in lattice spacing can be quantified, providing information about the lattice strain.

Crystal Size: Crystal size determination in XRD involves estimating the average size of the crystal domains, known as crystallites, within a material. This is typically done by analyzing the peak broadening observed in the XRD pattern. The Scherrer equation is commonly used to calculate the crystallite size based on the peak broadening information. The equation relates the peak broadening to the average crystallite size, taking into account factors such as the wavelength of the X-rays and the peak shape.

The calculation of lattice strain and crystal size from X-ray diffraction (XRD) data involves analyzing the peak positions and peak broadening in the diffraction pattern. Here's a step-by-step guide on how to perform these calculations:

Peak Positions: Determine the 2θ angles at which the diffraction peaks occur in the XRD pattern. These angles represent the positions of the peaks and are related to the spacing between the crystal lattice planes.

Bragg's Law: Apply Bragg's Law, which relates the peak positions to the lattice spacing (d-spacing) and the wavelength (λ) of the X-rays. The equation is given by:

$$n\lambda = 2d \sin(\theta)$$

where n is the order of the diffraction peak, λ is the X-ray wavelength, d is the lattice spacing, and θ is the Bragg angle.

Lattice Strain Calculation: Calculate the lattice strain (ε) using the relation:

$$\varepsilon = (d - d_0) / d_0$$

where $d_0$ is the lattice spacing of the unstrained crystal and d is the measured lattice spacing from the XRD data.

Peak Broadening Analysis: Measure the full width at half maximum (FWHM) of the diffraction peaks. The FWHM represents the broadening of the peaks and can be measured in terms of $2\theta$ or the corresponding angle at half maximum intensity.

Scherrer Equation for Crystal Size: Estimate the average crystallite size (D) using the Scherrer equation:

$$D = K\lambda / (\beta \cos \theta)$$

where D is the crystallite size, K is the Scherrer constant (typically taken as 0.9), $\lambda$ is the X-ray wavelength, $\beta$ is the FWHM after instrumental broadening corrections, and $\theta$ is the Bragg angle.

Instrumental Broadening Correction: If there is significant instrumental broadening, subtract the instrumental contribution from the FWHM. Instrumental broadening arises from the X-ray source, sample geometry, and XRD instrument characteristics.

Strain-Broadening Analysis: Analyze the peak broadening in terms of strain broadening and size broadening contributions. The strain broadening arises from lattice strain, while the size broadening is related to the finite size of the crystallites.

Strain and Size Broadening Separation: Depending on the specific contributions and the available data, various methods can be used to separate the strain and size broadening components, such as the Williamson-Hall or Warren-Averbach methods. These techniques involve analyzing the peak shape and fitting the experimental data to appropriate models.

Table 5.5: Linear fit data of Inconel 718

| θ (radians) | FWHM (rad) | β cosθ | 4 sinθ |
|---|---|---|---|
| 0.447189395 | 0.006245 | 0.005631 | 1.729732 |
| 0.498782375 | 0.006731 | 0.005911 | 1.913426 |
| Theta (radians) | FWHM rad | β cosθ | 4 sinθ |

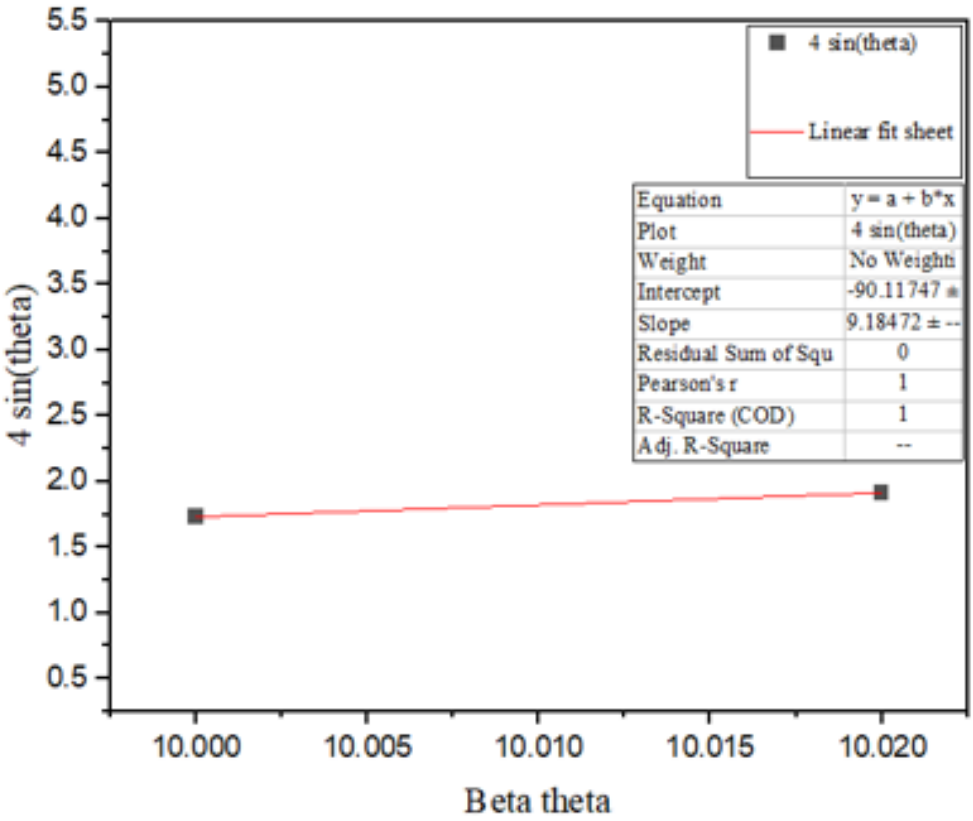


Fig 5.6: Linear fit of Inconel 718

On calculation, COD($R^2$) = 0.92139894451

Crystal size = 39 nm

And, Lattice strain = $3.658584 \times 10^{-4}$

Table 5.6: Linear fit data of Ti6Al4V

| θ (radians) | FWHM (rad) | β cosθ | 4 sinθ |
|---|---|---|---|
| 0.360985 | 0.004067 | 0.003805 | 1.412785 |
| 0.39325 | 0.003697 | 0.003414 | 1.532768 |
| 0.40511 | 0.006521 | 0.005993 | 1.576478 |
| 0.413523 | 0.00425 | 0.003892 | 1.607351 |
| 0.424557 | 0.000223 | 0.000203 | 1.647669 |

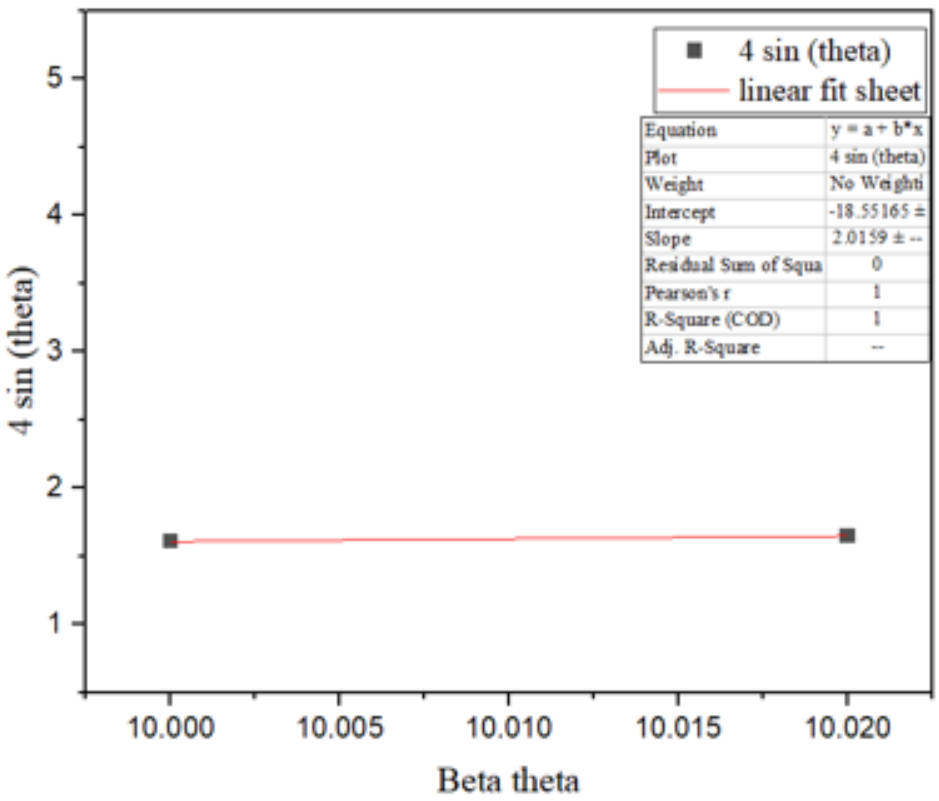


Fig 5.7: Linear fit of Ti6Al4V

On calculation, $COD(R^2) = 0.9090820251$

Crystal size = 74 nm

And, Lattice strain = $2.015954 \times 10^{-4}$

Table 5.7: Linear fit data of Inconel 718 weld region

| θ (radians) | FWHM (rad) | β cosθ | 4 sinθ |
|---|---|---|---|
| 0.433756294 | 0.00525903 | 0.004772 | 1.681129 |
| 0.446556714 | 0.00804719 | 0.007258 | 1.72745 |
| 0.466693886 | 0.00794334 | 0.007094 | 1.799745 |
| 0.42520933 | 0.02403283 | 0.021893 | 1.650046 |
| 0.412275916 | 0.00730612 | 0.006694 | 1.602782 |
| 0.1360074 | 0.00250315 | 0.00248 | 0.542354 |
| 0.522083917 | 0.00842942 | 0.007306 | 1.99475 |
| 0.547900042 | 0.00700453 | 0.005979 | 2.083583 |
| 0.605112022 | 0.01484926 | 0.012213 | 2.275417 |
| 0.637304446 | 0.00906524 | 0.007286 | 2.380125 |
| 0.658040266 | 0.00904342 | 0.007155 | 2.44627 |

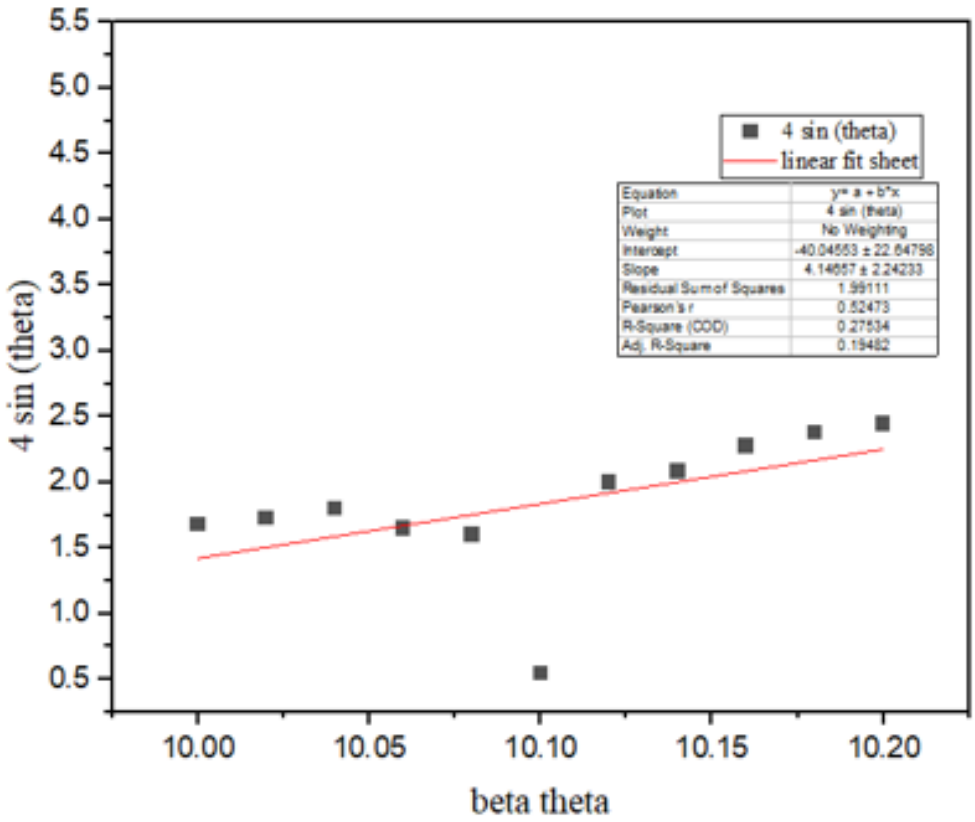


Fig 5.8: Linear fit of Inconel 718 weld region

On calculation, $COD(R^2) = 0.912359545$

Crystal size = 34 nm

And, Lattice strain = $4.125562 \times 10^{-4}$

Table 5.8: Linear fit data of Ti6Al4V weld region

| θ (radians) | FWHM (rad) | β cosθ | 4 sinθ |
|---|---|---|---|
| 0.40458504 | 0.008264 | 0.007597 | 1.574549 |
| 0.40542314 | 0.00843 | 0.007746 | 1.577631 |
| 0.40730888 | 0.007749 | 0.007115 | 1.584559 |
| 0.42288804 | 0.005607 | 0.005113 | 1.641583 |
| 0.44562994 | 0.007368 | 0.006648 | 1.724106 |
| 0.52108271 | 0.011149 | 0.009669 | 1.991278 |

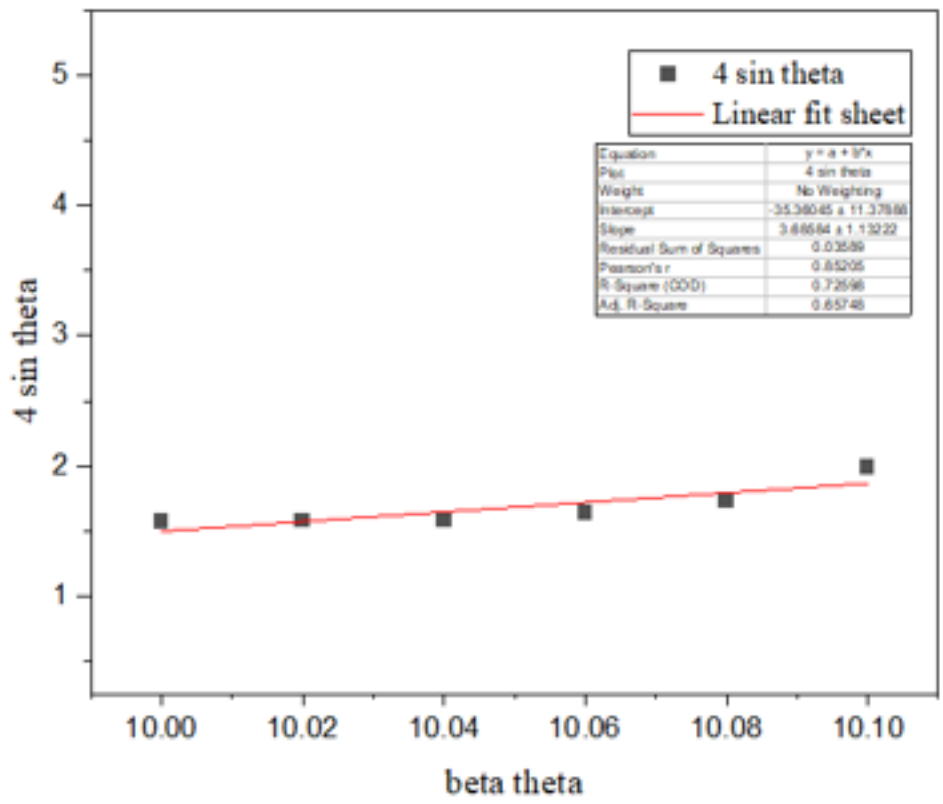


Fig 5.9: Linear fit of Ti6Al4V weld region

On calculation, $COD(R^2) = 0.959545123$

Crystal size = 39 nm

And, Lattice strain = $3.569584 \times 10^{-4}$

# CHAPTER 6
# RESULTS AND DISCUSSIONS

Inconel 718 is a nickel based superalloy which has high value of mechanical properties which increases its application in the aerospace and marine industries as same the Ti6Al4V, titanium alloy renowned for its strength-to-weight ratio, corrosion resistance, and biocompatibility. TIG welding offers excellent control over the welding process, producing high-quality and precise welds. In considering with the simulations with CATIA software the similar and dissimilar welds formed between Inconel 718 and Ti6Al4V alloys are tested for deformation, Von Mises, displacement and principal stress under the applied load of 100 N in the X-direction. The conclusions can be made that the similar welds formed between Inconel 718 and Ti6Al4V and dissimilar welds between Inconel 718 and Ti6Al4V has shown minimum, maximum and average value of displacement in mm is 0.0243, 0.04255 and 0.0324 respectively. The similar welds formed between Inconel 718 and Ti6Al4V and dissimilar welds between Inconel 718 and Ti6Al4V has shown minimum, maximum and average value of Von Mises stress in $Nm^2$ 1227.425023, 1223.390735 and 1160.915697respectively. The similar welds formed between Inconel 718 and Ti6Al4V and dissimilar welds between Inconel 718 and Ti6Al4V has shown minimum, maximum and average value of principal stress in $Nm^2$ is 5490.66588, 2767.521524, 6749.363715.

In case of the experimental procedure, successful strong welds can be generated between the similar alloy welds but in case of the dissimilar metal welding between Inconel 718 and Ti6Al4V the weld joints are becoming more brittle in nature and which succeeds in the breakage of the weld. On conducting the XRD analysis we can conclude that there occurs the formation of intermetallic compounds $Ni_3Ti$ and $Ti_2Ni$. The L12 structure is the crystal structure of $Ni_3Ti$. It has a face-centered cubic (FCC) configuration and is a member of the cubic crystal system. A particular configuration of Ni and Ti atoms within the crystal lattice defines the L12 structure. As an intermetallic complex, $Ni_3Ti$ separates from pure metals to form a distinct phase. When compared to the individual constituent metals, intermetallic complexes frequently display distinctive characteristics. $Ti_2Ni$ is another name for an intermetallic compound that is created when titanium (Ti) and nickel (Ni) are combined. The Laves phase structure is a particular crystal structure seen in crystals. It has a close-packed hexagonal (CPH) configuration and is a member of the hexagonal crystal system. Atomic layers

within the crystal lattice that alternate between being hexagonal and cubic define the Laves phase structure. As an intermetallic complex, $Ti_2Ni$ separates from the pure metals into a distinct phase. Brittle behavior has been seen with $Ti_2Ni$. The formation of these to intermetallic brittle compounds is the major reason of breakage of dissimilar metal welding between Inconel 718 and Ti6Al4V.

# CHAPTER 7
# CONCLUSIONS

The project's main objective was to employ CATIA's simulation-based technique to weld Inconel 718 and Ti6Al4V, two dissimilar metals. With the major disparities in material characteristics and mechanical behavior between the two alloys, the goal was to evaluate the viability and efficacy of the welding process. The simulation-based methodology was used to examine and assess the welds' varied mechanical properties. This includes the primary stress distribution, the Von Mises stress distribution, and the deformation in the welded region.

The simulation findings showed that Inconel 718 and Ti6Al4V had the ability to be successfully welded together as dissimilar metals. But we were unable to produce a satisfactory weld between Inconel 718 and Ti6Al4V during the experimental study that was carried out. After performing an XRD investigation on the failed weld, we discovered that the intermetallic brittle compounds Ni3Ti and Ti2Ni are what cause the weld to fracture. The use of interlayers or filler materials to strengthen joints and decrease the production of brittle intermetallic compounds was also examined by this experiment. To ensure accuracy and reliability, it is crucial to highlight that simulation results should be validated through experimental testing. The mechanical characteristics of the welded joints, including their tensile strength, fatigue resistance, and corrosion behavior, should be confirmed through additional research. A more thorough understanding of the welds performance and applicability for real-world applications would result from future experimental validation.

Overall, this study demonstrated the ability of simulation-based methods, particularly in CATIA, to direct the welding process for different metals. Engineers and researchers can improve welding parameters, eliminate the need for expensive and time-consuming trial-and-error trials, and obtain insightful knowledge into the behavior of the welding process by utilizing the power of computer-aided design and analysis tools. The results of this study add to the body of information about dissimilar metal welding and serve as a starting point for more study and advancement in this area.

# REFERENCE


1. K.H. Song, K. Nakata 2010, Microstructural and mechanical properties of friction-stir-welded and post-heat-treated Inconel 718 alloy.
2. K. Devendranath Ramkumar N, B. Monoj Kumar, M. Gokul Krishnan, Sidarth Dev, Aman Jayesh Bhalodi, N. Arivazhagan, S. Narayanan, 2015 Studies on the weldability, microstructure and mechanical properties of activated flux TIG weldments of Inconel 718.
3. Guangxu Yana , Ming Jen Tanb , Alexandru Crivoic , Feng Lid , Sandeep Kumare and Chern How Nicholas Chia, 2017, Improving the mechanical properties of TIG welding Ti-6Al-4V by post weld heat treatment.
4. Xiao-Long Gao & Jing Liu & Lin-Jie Zhang,2018, Dissimilar metal welding of Ti6Al4V and Inconel 718 through pulsed laser welding-induced eutectic reaction technology
5. K. C. Ganesh , M. Vasudevan , K. R. Balasubramanian , N. Chandrasekhar & P. Vasantharaja, 2014, Thermo-mechanical Analysis of TIG Welding of AISI 316LN Stainless Steel.
6. Prashant Sagar* , Deepak Kumar Gope and Somnath Chattopadhyaya,2018, Thermal analysis of TIG welded Ti-6Al-4V plates using ANSYS.
7. Antony Solomon.S, Deepak. R, Aravinthan. G, Kishore Kumar. M, 2018, Simulation and Modeling of the Effect of Welding Process Parameters of Inconel 625.
8. Shehbaz, Tauheed, Junaid, Massab, Khan, Fahd Nawaz and Haider, Julfikar, 2022, Dissimilar P-TIG Welding between Inconel 718 and Commercially Pure Titanium Using Niobium Interlayer.
9. Jing Liu, Huan Liu, Xiao-Long Gao , Haokui Yu, 2019, Microstructure and mechanical properties of laser welding of Ti6Al4V to Inconel 718 using Nb /Cu interlayer.
10. Timo Rautio, Atef Hamada, Jarmo Mäkikangas, Matias Jaskari, Antti Järvenpää,2019, Laser welding of selective laser melted Ti6Al4V: Microstructure and mechanical properties.
11. Chao Chen, Chenglei Fan∗ , Xiaoyu Cai, Sanbao Lin, Zeng Liu, Qingkai Fan, Chunli Yang,2019, Investigation of formation and microstructure of Ti-6Al-4V weld bead during pulse ultrasound assisted TIG welding.

12. C. Mukundhan , P. Sivaraj , V. Balasubramanian, Tushar Sonar , Vijay Petley , Shweta Verma,2023, Effect of friction pressure on microstructure and tensile properties of linear friction welded Tie6Ale4V alloy joints.
13. Balrm Yelamasetti , G Sai Adithya , R Sri Ramadevi , Pankaj Sonia , Kuldeep K. Saxena , Naveen Kumar P , Sayed M. Eldin , Fatima Hiader Kutham Al- kafaji, 2023, Metallurgical, mechanical and corrosion behaviour of pulsed and constant current TIG dissimilar welds of AISI 430 and Inconel 718.
14. E. Ahmadi, M. Goodarzi, 2022, Mechanical response and wear behavior of graphene reinforced inconel 718 composite produced via hybrid accumulative roll bonding and gas tungsten arc welding process.
15. Jacek Gorka,Wojciech Jamrozik, Marta Kiel-Jamrozik, 2023, The effect of TIG welding on the structure and hardness of butt joints made of Inconel 718
16. Chaitanya T K and Harinadh Y B, Simulation of Welding for Dissimilar Metals using Abaqus, 2016.
17. Ahmed Y M, Salleh K, Sahari M and Ishak M, Welding of Titanium (Ti-6Al-4V) Alloys, 2012.
18. Akbari Mousavi. S.A.A, R. Miresmaeili., Experimental and numerical analyses of residual stress distributions in TIG welding process for 304L stainless steel, 2008.
19. Amudala Nata Sekhar Babu, Finite Element Simulation of Hybrid Welding Process for Welding 304 Austenitic Stainless Steel Plate, 2012.
20. Dean Deng, Hidekazu Murakawa, Prediction of welding distortion and residual stress in a thin plate butt-welded joint, 2008
21. Goldak.J.A, B. Chakravarti and M. J. Bibby, A new finite element model for welding heat sources, Metallurgical Transactions, 2015.
22. Deng D, Murakawa H, Liang W, Numerical simulation of welding distortion in large structures, 2007.
23. Rathod M S S, Gaikwad S P and Katikar N S, Finite Element Model for the Effect of Heat Input & Speed on Residual Stress during Welding, 2013.
24. Chaudhari R, Ingle A and Kalita K, Stress Analysis of Dissimilar Metal Weld between Carbon Steel and Stainless Steel formed by Transition Grading Technique, 2015.
25. Lu F, Tang X, Yu H and Yao S, Numerical simulation on interaction between TIG welding arc and weld pool, 2006.
26. Zoeram AS, Mousavi SAAA, Laser welding of Ti-6Al-4V to nitinol, 2014.

27. Zoeram AS, Mousavi SAAA, Effect of interlayer thickness on microstructure and mechanical properties of as welded Ti6Al4V/ Cu/NiTi joints, 2014.
28. Casalinoa G, Guglielmia P, Lorussoa VD, Mortellob M, Peyrec P, Sorgenteda D, Laser offset welding of AZ31B magnesium alloy to 316 stainless steel, 2017.
29. Ramkumara KD, Abrahama WS, Viyasha V, Arivazhagana N, Rabelb AM, Investigations on the microstructure, tensile strength and high temperature corrosion behaviour of Inconel 625 and Inconel 718 dissimilar joints, 2017.
30. Zhang Y, Sun DQ, Gu XY, Li HM, A hybrid joint based on two kinds of bonding mechanisms for titanium alloy and stainless steel by pulsed laser welding, 2016.
31. Esfahani MRN, Coupland J, Marimuthu S, Numerical simulation of alloy composition in dissimilar laser welding, 2015.
32. Sanjeev Kumar, Swati Gangwar, Flexural analysis of green composite material using CATIA V5 for tool carrier, 2021.
33. Singh A K, Dey V and Rai R N, Techniques to improveweld penetration in TIG welding, 2017.
34. Chen HC, Pinkerton AJ, Li L,Fiber laser welding of dissimilar alloys of Ti6Al4Vand Inconel 718 for aerospace applications, 2011.
35. Chatterjee S, Abinandanan TA, Reddy GM, Chattopadhyay K, Microstructure formation in dissimilar metal welds: electron beam welding of Ti/Ni, 2016.
36. Ramkumara KD, Abrahama WS, Viyasha V, Arivazhagana N, Rabelb AM, Investigations on the microstructure, tensile strength and high temperature corrosion behaviour of Inconel 625 and Inconel 718 dissimilar joints, 2017.
37. Mei YP, Liu YC, Liu CX, Li C, Yu LM, Guo QY, Li HJ, Effect of base metal and welding speed on fusion zone microstructure and HAZ hot-cracking of electron-beam welded Inconel 718, 2016.
38. Satoh G, Yao LY, Qiu CA, Strength and microstructure of laser fusion-welded Ti-SS dissimilar material pair, 2013.
39. T. Morita, K. Hatsuoka, T. Iizuka, K. Kawasaki, Strengthening of Ti-6Al-4V alloy by short-time duplex heat treatment, 2005.
40. X. Demulsant, J. Mendez, Influence of environment on low cycle fatigue damage in Ti6Al4V and Ti 6246 titanium alloys, 2006.
41. N.K. Babu, S.G.S. Raman, R. Mythili, S. Saroja, Correlation of microstructure with mechanical properties of TIG weldments of Ti–6Al–4V made with and without current pulsing, 2007.